วัสดุไดโอดอินทรีย์เปล่งแสงจากอนุพันธ์ไตรเอซาทรุกซีน
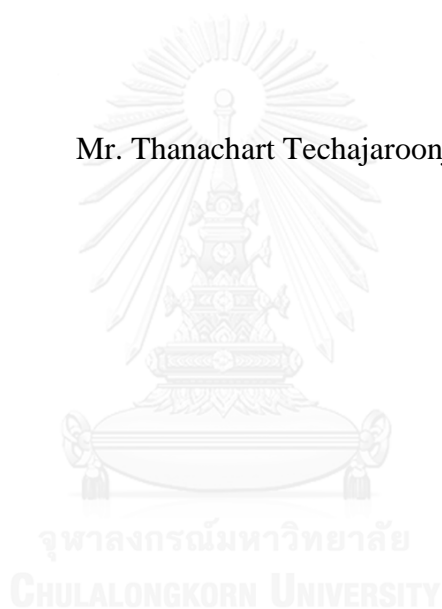
นายธนชาติ เตชจรูญจิตร

วิทยานิพนธ์นี้เป็นส่วนหนึ่งของการศึกษาตามหลักสูตรปริญญาวิทยาศาสตรมหาบัณฑิต
สาขาวิชาเคมี ภาควิชาเคมี
คณะวิทยาศาสตร์ จุฬาลงกรณ์มหาวิทยาลัย
ปีการศึกษา 2557
ลิขสิทธิ์ของจุฬาลงกรณ์มหาวิทยาลัย

ORGANIC LIGHT-

EMITTING DIODE MATERIAL FROM TRIAZATRUXENE DERIVATIVES

Mr. Thanachart Techajaroonjit

A Thesis Submitted in Partial Fulfillment of the Requirements

for the Degree of Master of Science Program in Chemistry

Department of Chemistry

Faculty of Science

Chulalongkorn University

Academic Year 2014

Thesis Title	ORGANIC LIGHT-EMITTING DIODE MATERIAL FROM TRIAZATRUXENE DERIVATIVES
By	Mr. Thanachart Techajaroonjit
Field of Study	Chemistry
Thesis Advisor	Associate Professor Paitoon Rashatasakhon, Ph.D.
Thesis Co-Advisor	Associate Professor Vinich Promarak, Ph.D.

Accepted by the Faculty of Science, Chulalongkorn University in Partial Fulfillment of the Requirements for the Master's Degree

.... Dean of the Faculty of Science
(Professor Supot Hannongbua, Dr.rer.nat.)

THESIS COMMITTEE

.... Chairman
(Associate Professor Vudhichai Parasuk, Ph.D.)

.... Thesis Advisor
(Associate Professor Paitoon Rashatasakhon, Ph.D.)

.... Thesis Co-Advisor
(Associate Professor Vinich Promarak, Ph.D.)

.... Examiner
(Associate Professor Mongkol Sukwattanasinitt, Ph.D.)

.... External Examiner
(Assistant Professor Pannraphat Takolpuckdee, Ph.D.)

ธนชาติ เตชจรูญจิตร : วัสดุไดโอดอินทรีย์เปล่งแสงจากอนุพันธ์ไตรเอซาทรุกซีน (ORGANIC LIGHT-EMITTING DIODE MATERIAL FROM TRIAZATRUXENE DERIVATIVES) อ.ที่ปรึกษาวิทยานิพนธ์หลัก: รศ. ดร. ไพฑูรย์ รัชตะสาคร, อ.ที่ปรึกษาวิทยานิพนธ์ร่วม: รศ. ดร. วินิช พรมอารักษ์, 70 หน้า.

สารประกอบจากอนุพันธ์ของไตรเอซาทรุกซีน-ไพรีนชนิดใหม่จำนวนสองชนิด (TAT1 และ TAT2) สามารถสังเคราะห์ได้สำเร็จโดยผ่านปฏิกิริยาไซโคลไตรเมอร์ไรด์เซชันผ่านโบรมีน และปฏิกิริยาซูซูกิครอสคัปปลิงด้วยไพรีนโบโรนิกเอซิด หมู่แทนที่ในตำแหน่งไนโตรเจน 2-เอ ทิลเฮกซิลและเบนซิลสามารถป้องกันการจับตัวของสารโดยการเกิดการซ้อนกันของพายออบิทัล ในสารละลายคลอโรฟอร์มสารดังกล่าวดูดกลืนแสงและคายแสงในช่วงความยาวคลื่น 344-351 และ 472-483 นาโนเมตรตามลำดับ จากการศึกษาสมบัติทางเคมีไฟฟ้าโดยใช้ไซคลิกโวลแทมเม ตรีพบว่าสารทั้งสองมีออบิทัลสูงสุดที่มีอิเล็กตรอนบรรจุอยู่ที่ -5.15 และ -5.16 อิเล็กตรอนโวลต์ ตามลำดับ ในขณะที่มีออบิทัลต่ำสุดที่ไม่มีอิเล็กตรอนบรรจุอยู่ที่ -1.74 และ -1.68 อิเล็กตรอน โวลต์ตามลำดับ นอกจากนี้สารทั้งสองยังมีเสถียรภาพทางความร้อนที่ดีเยี่ยม โดยมีค่าอุณหภูมิทราน ซิชันแก้วและมีอุณหภูมิการสลายตัวสูงกว่า 230 และ 305 องศาเซลเซียสตามลำดับ เมื่อนำ สารประกอบ TAT1 และ TAT2 ไปขึ้นรูปผนวกเป็นชั้นส่งผ่านประจุบวกในอุปกรณ์ไดโอด อินทรีย์เปล่งแสงที่มีอินเดียมทินออกไซด์เป็นแอโนด มีลิเธียมฟลูออไรด์เคลือบบนอะลูมินัมเป็น แคโทด และมีอะลูมินัมไตรไฮโดรควิโนลีนเป็นชั้นเปล่งแสง พบว่าอุปกรณ์ที่มีสาร TAT2 เป็นชั้น ส่งผ่านประจุบวกมีประสิทธิภาพมากกว่าถึงสามเท่าเมื่อเปรียบเทียบกับ TPD ซึ่งเป็นสารมาตรฐาน ที่มีหน้าที่ส่งผ่านประจุบวก โดยจะให้แสงสีเขียวที่มีค่าความสว่างสูงสุดที่ 31,971 แคนเดลาต่อ ตารางเมตร ที่ 5.2 โวลต์ โดยมีค่าศักย์ไฟฟ้าเริ่มต้น 2.6 โวลต์

ภาควิชา	เคมี	ลายมือชื่อนิสิต	....
สาขาวิชา	เคมี	ลายมือชื่อ อ.ที่ปรึกษาหลัก	....
ปีการศึกษา 2557		ลายมือชื่อ อ.ที่ปรึกษาร่วม	....

5571987023 : MAJOR CHEMISTRY

KEYWORDS: TRIAZATRUXENE / PYRENE / HOLE-TRANSPORTING / C-N COUPLING / ORGANIC LIGHT-EMITTING DIODE / ELECTROLUMINESCENCE

THANACHART TECHAJAROONJIT: ORGANIC LIGHT-EMITTING DIODE MATERIAL FROM TRIAZATRUXENE DERIVATIVES. ADVISOR: ASSOC. PROF. PAITOON RASHATASAKHON, Ph.D., CO-ADVISOR: ASSOC. PROF. VINICH PROMARAK, Ph.D., 70 pp.

Two new symmetrical pyrenyl triazatruxene derivatives (TAT1 and TAT2) were successfully synthesized *via* Br_2-catalyzed cyclotrimerization of indole and Suzuki cross-coupling with pyrene-1-boronic acid. The substitution of the -NH position by 2-ethylhexyl and benzyl groups could prevent the aggregation by pi-stacking. These compounds exhibited maximum absorption and emission around 344-351 nm and 472-483 nm in $CHCl_3$ solution, respectively. The electrochemical investigation by cyclic voltammetry (CV) suggested that the HOMO energy level of TAT1 and TAT2 were at -5.15 and -5.16 eV, while the LUMO energy level were at -1.74 and -1.68 eV, respectively. Both compounds exhibited excellent thermal stabilities with high glass transition temperatures (T_g) and decomposition temperature (T_d) above 230 ℃ and 305 ℃, respectively. OLED devices structures ITO/PEDOT:PSS/TAT1 or TAT2/Alq_3/LiF:Al were fabricated to study their hole-transporting properties. The performance of TAT2 was three-time better than that of TPD, which exhibited a bright green emission with a maximum luminescence of 31,971 cd/m^2 at 5.2 V and a turn-on voltage of 2.6 V.

Department:	Chemistry	Student's Signature
Field of Study:	Chemistry	Advisor's Signature
Academic Year:	2014	Co-Advisor's Signature

ACKNOWLEDGEMENTS

CONTENTS

LIST OF FIGURES

จุฬาลงกรณ์มหาวิทยาลัย
CHULALONGKORN UNIVERSITY

LIST OF SCHEMES

จุฬาลงกรณ์มหาวิทยาลัย
CHULALONGKORN UNIVERSITY

LIST OF TABLES

LIST OF ABBREVIATIONS

A	Ampere
Å	Angstrom
Acetone-d6	Deuterated acetone
Alq_3	Tris(8-hydroxyquinoline)aluminium
Al	Aluminium
^{o}C	Degree of celsius
cm^2	Square centimeter
Ca	Calcium
cd	Candela
$CDCl_3$	Dueterated chloroform
CH_2Cl_2	Methylene chloride
CRT	Cathode ray tube
CV	Cyclic voltammetry
d	Doublet
dd	Doublet of doublet
DSC	Differential scanning colorimeter
EMMs	Emitting materials
EL	Electroluminescent
EML	Emitting layer
ETL	Electron-transporting layer
EtOAc	Ethyl acetate
eV	Electron volt
g	Gram (s)

h	Hour
HOMO	Highest occupied molecular orbital
HRMS	High resolution mass spectroscopy
H_2SO_4	Sulfuric acid
HTL	Hole-transporting layer
HTMs	Hole-transporting materials
Hz	Hertz
ITO	Indium tin oxide
J	Coupling constant
K_2CO_3	Potassium carbonate
LCD	Liquid crystal display
LED	Light-emitting diode
lm	Lumen
LiF	Lithium fluoride
LUMO	Lowest unoccupied molecular orbital
Mg	Magnesium
m^2	Square meter
m	Multiplet
mg	Milligram (s)
$MgSO_4$	Magnesium sulfate
min	Minute (s)
mL	Milliliter (s)
mmol	Millimole
M	Molar
MS	Mass spectroscopy

m.p.	Melting point
nm	Nanometer (s)
NMR	Nuclear magnetic resonance
OLED	Organic light-emitting diode
$Pd(PPh_3)_4$	Tetrakis(triphenylphosphine)palladium
ppm	Parts per million
PL	Photoluminescent
s	Singlet
t	Triplet
T_g	Glass transition temperature
TGA	Thermo gravimetric analysis
THF	Tetrahydrofuran
TLC	Thin layer chromatography
V	Volt
W	Watt
%	Percent
δ	Chemical shift
ε	Molar absorptivity
λ	Wavelength
Φ	Fluorescence quantum yield

CHAPTER I

INTRODUCTION

1.1 Introduction to OLEDs

Nowadays, research on organic light-emitting diodes (OLEDs) has been continuously developed during the last few decades. OLED display has thus become a theme of interest due to its advantages such as properties for large area, flexible, lightweight and energy efficient optoelectronic [1].

Prior to the OLEDs, many display technologies such as cathode ray tube (CRT), liquid crystal displays (LCD), plasma displays were leading in the display marget. All of them have their limitations, for example, bulkiness, low viewing angle, color tenability, etc. The essential requirements of present generation displays are reproduction of good light quality, brightness contrast, improve color variation, high resolution, low weight, reduction in thickness, reduction in cost, low power consumption. Therefore, OLEDs have been improved and developed to fulfill these requirements.

| (a) | (b) | (c) | (d) |
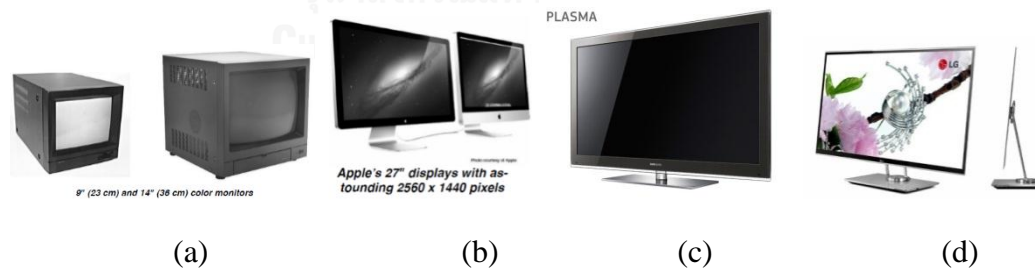
Figure 1.1 (a) CRT, (b) LCD, (c) plasma, and (d) OLED displays in computer monitor [2]

From **Figure 1.2**, OLED display shows better quality in brightness and contrast, which are important things to develop the next generation of flat panel displays over the LCD displays.
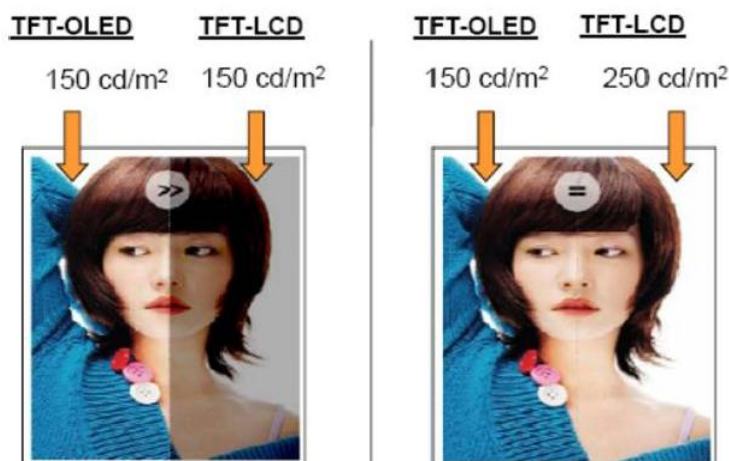
Figure 1.2 Comparison of brightness and contrast between OLED and LCD display [3]

In 1987, Tang and Van Slyke reported the first diode device at Kodak. They made a double layered device containing active "small molecules" with low-voltage (<10V) based on thin films of ~100 nm Alq_3 with good brightness (>1000 cd/m^2) and respectable luminous efficiency (1.5 lm/W) [4].
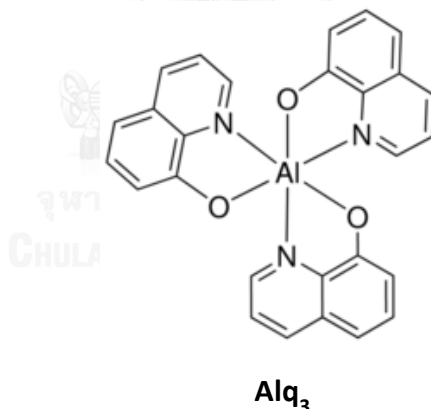
Alq$_3$

Figure 1.3 Chemical structure of Alq_3

1.2 Structure and operation of OLED

Structure of different OLEDs is shown in Figure **1.4**. A single-layer OLED is made of a single organic layer sandwiched between the cathode and the anode. This layer must not only possess high quantum efficiency for photoluminescence, but the layer must also have good hole and electron transport properties. In a two-layer OLED, one organic layer is specifically chosen to transport holes and the other layer

is chosen to transport electrons. Recombination of the hole-electron pair takes place at the interface between the two layers, which generates electroluminescence. In a three-layer OLED, an additional layer is placed between the hole transporting layer and the electron transporting layer. The emitting layer is primarily the site of hole-electron recombination and thus for electroluminescence. This cell structure is useful for emissive materials that do not possess high carrier transport properties. In a multi-layer OLED an electron injection layer is also included. Introduction of multi-layer device structure eliminates the charge carrier leakage as well as exciton quenching, as excited states are generally quenched at the interface of the organic layer and the metal. Multi layer OLEDs consist of different layers namely ITO glass plate, hole injection layer (HIL), hole transport layer (HTL), emitting layer (EML), electron transporting layer (ETL) and anode.
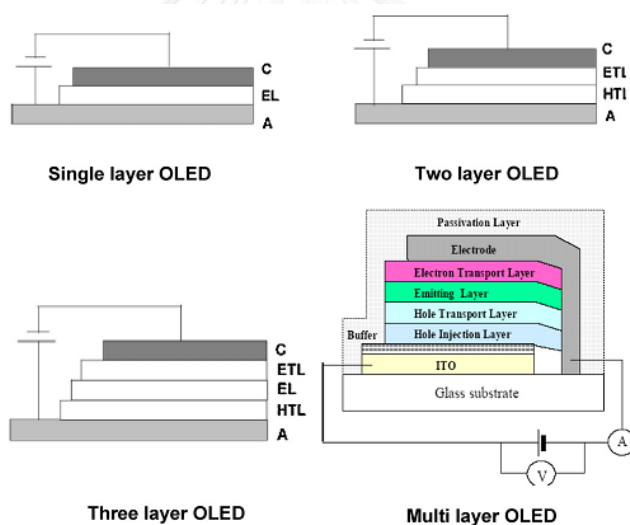
Figure 1.4. Structure of different OLEDs. Where C = cathode (typically aluminum); EL = emitting layer; ETL = electron transport layer; HTL = hole transport layer; HIL = hole injection layer; A = anode small molecules

Multi layer OLED device have several layers, which differ in their properties. When voltage is applied across the layers of OLED, current flows through the device. Therefore, the cathode gives electrons to the emissive layer and holes are injected from the anode, forming exciton pairs in the emissive layer. When the charges in

exciton pairs are combined, they give rise to light emission. The color of the light depends on the type of organic molecule in the emissive layer. Emission color is basically determined by the energy difference of HOMO and LUMO of the emitting organic material. The intensity or brightness of the light depends on the amount of electrical current applied. Consequently by changing these active materials the emission color can be varied across the entire visible spectrum. Light emitting mechanism from an OLED device is shown in **Figure 1.5**.
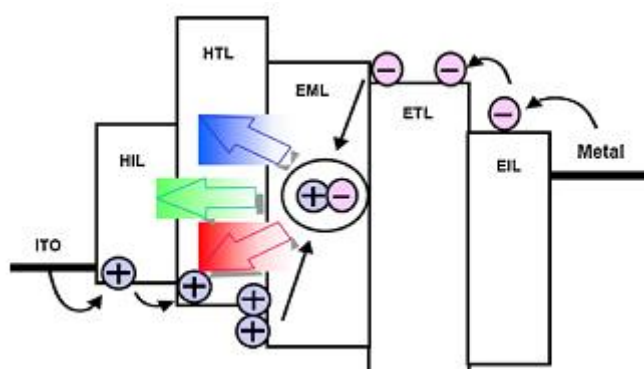
Figure 1.5 Light-emitting mechanism in an OLED device

1.3 Organic electroluminescent materials

Organic light emitting materials have been attracting attention of researchers from industry and academic institutions owing to their applications in OLEDs [5]. The reason is that the numerous organic materials with high fluorescence quantum efficiencies in the visible light. OLED materials can be categorized into polymeric materials and low molecular-weight materials.

1.3.1   Conjugated polymers

The first polymeric light-emitting diode based on a luminescent conjugated polymer was demonstrated in 1990 by Burroughes and co-workers at Cambridge University. The polymer was PPV, which is luminescent but not soluble in organic solvents. The PPV film was prepared from its solution-processable precursor polymer by thermal conversion. Ultra-thin, dense and homogenous film of PPV was formed on a suitable substrate, which had been pre-coated with a transparent bottom

electrode. The device was completed by the deposition of a top electrode on top of the PPV film. Substantial charge injection was achieved with a DC voltage bias of just below 14 V, with indium oxide electrode positively biased with respect to the aluminum electrode. However, the quantum efficiency of the PPV devices was only 0.05%, much lower than the estimated photoluminescence (PL) quantum yield of about 8% for PPV. The results of the Cambridge group were quickly confirmed by Braun and Heeger at UC Santa Barbara, with improved material processability and device performance [6, 7]. The intensive research and development activity in polymer LEDs mirrored that of organic LEDs in recent years.
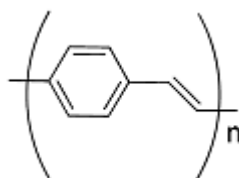
Figure 1.6 Chemical structure of Poly(p-phenylenevinylene) (PPV)

1.3.2   Low molecular-weight materials

The work pioneered by Tang and Van Slyke initiates recent improvements of the OLED device efficiency and durability. For the fabrication of highly stable OLED, low molecular weight materials with specific optical and electronic properties such as fluorescence, energy levels, charge mobility, etc., and high morphology and thermally stable are required [8]. The thermal stability of materials used in OLED is the one of the significant factors of the device durability. Under thermal stress, most organic materials tend to turn into the thermodynamically stable crystalline state, which leads to device failure [9]. A considerable amount of evidence indicates that an amorphous thin film with a high glass transition temperature (T_g) is more stable to heat damage [10]. For the organic materials in OLED, high thermal stability, especially high T_g, excellent film formability are essentially needed.

1.4 Hole transporting materials (HTMs)

The hole transporting materials play a key role in transporting holes and prevent electrons get to the other side of the electrode without recombination with holes. The HTM should be stable in the radical cationic form and easily oxidized. The typical HTMs are 4,4′-bis-[N-(1-naphthyl)-N-phenyl- amino]-biphenyl (NPB) [11-14] and N,N′-diphenyl-N,N′-bis(3-methylphenyl)-1,1′-biphenyl-4,4′-diamine (TPD) [15-19] which are widely used in OLED. The molecular structures are shown in **Figure 1.7**. They have an excellent hole transporting properties. However, they have low glass transition temperature (T_g) which affect the morphology at high operating temperature.
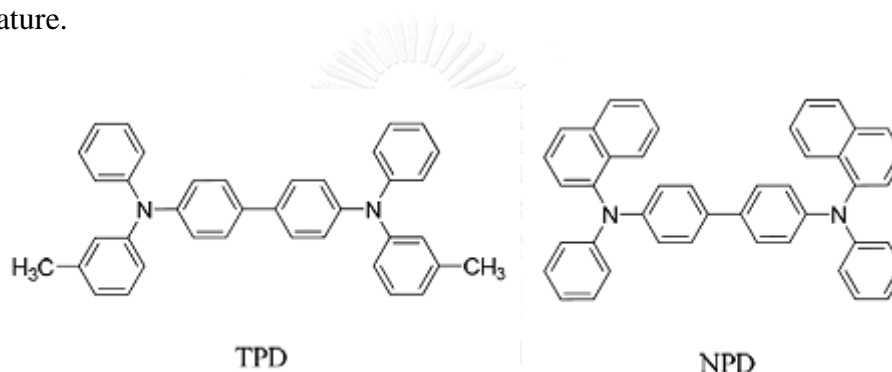
Figure 1.7 Chemical structures of NPB and TPD

1.5 Emitting materials (EMMs)

Organic fluorescence compounds are used as the emitter in OLED device. The fluorescence principle is described by the Jablonski diagram in **Figure 1.8**.
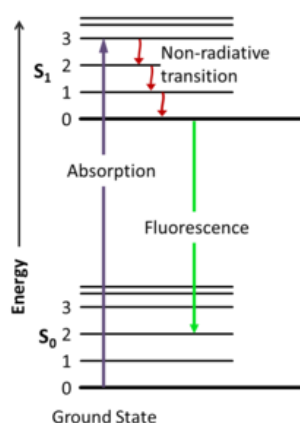
Figure 1.8 Jablonski diagram [20]

The requirements for full-color OLED display are consist of red, blue and green emitter to obtain a variety of colors by a combination of red, blue and green light. For example, the red emitter 4-(dicyanomethylene)-2-methyl-6-[4-(dimethyl-aminostyryl)-4H-pyran] (DCM) [21], a green emitter tris(8-hydroxyl-quinoline) aluminum (Alq₃) [12, 22] and blue emitters NPD and polyfluorene (PF) derivatives (**Figure 1.9**) [23, 24].
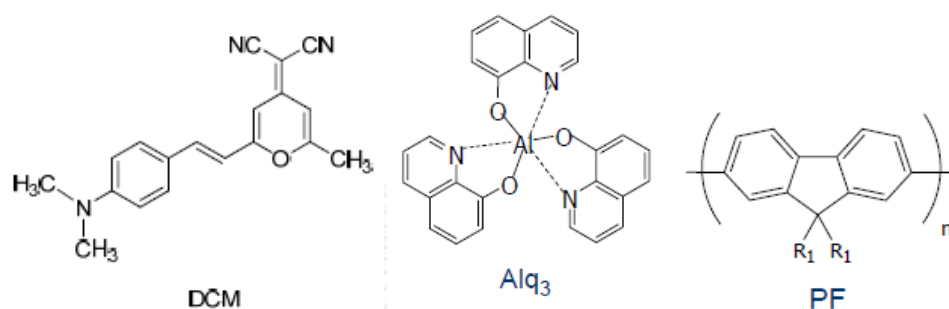
Figure 1.9 Chemical structures of DCM, Alq₃ and PF derivatives

One of the measure problems in OLEDs is its low efficiency. Various techniques are used to improve the efficiency of OLED devices. An important aspect of host–guest systems is the choice of host and guest materials for both single and multidoped systems [25, 26]. The energy transfer from host to guest can be either Förster type energy transfer or Dexter type charge transfer or due to the formation of excimer or exciplex. The primary conditions for such energy transfers are overlap of the emission spectrum of the host and absorption spectrum of the guest (**Figure 1.10**). Therefore, the host material is always one with emission at higher energies, generally a blue-emitting material. The example of host materials that widely used are poly(*N*-vinylcarbazole) (PVK), 1,1,4,4-tetraphenyl-1,3-butadiene (TPD), 4,4',*N,N*'-dicarbazole-biphenyl (CBP) or 4,4'bis(*N*-(1-naphthyl)-*N*-phenyl-amino)-biphenyl (α-NPD).
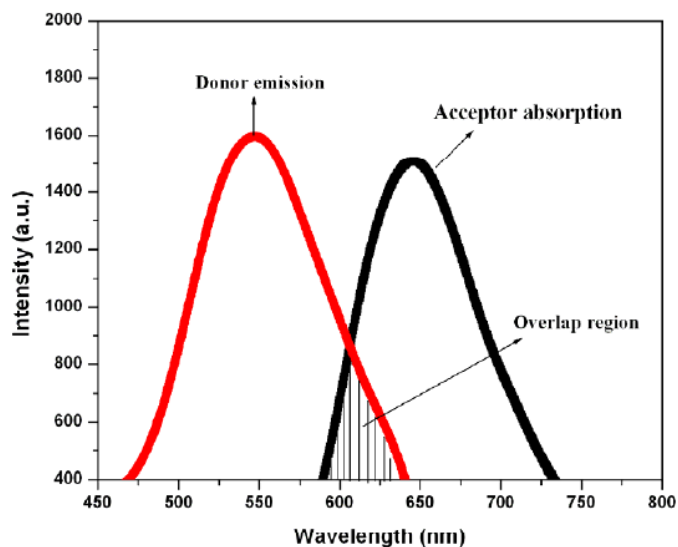
Figure 1.10 Spectral overlapping between emission of donor and absorption of acceptor [27]

1.6 OLED core fabrication technologies

OLED devices can be fabricated in two ways namely vacuum deposition technique and solution techniques including spin coat technique, ink jet technique, and casting, etc [28, 29].

Vacuum deposition technique is the widely used technique of thin film deposition. The material is evaporated in vacuum. Then, the vacuum allows the vapor particles to go directly to the substrate and condense back to solid state. Therefore, this technique is suitable only for volatile and thermally stable materials. However, it takes more time to reach high vacuum state and is difficult to deposit over large area.

On the other hands, solution techniques offer several advantages over vacuum deposition such as easily fabrication procedure, large area coverage and low power consumption. The simplest method for solution casting technique is using the centrifuge force by dropping small amount of the solution onto spinning head and spinning the solution, respectively. The centrifuge force will spread the solution into thin film layer on the top of substrate.

1.7 Literature reviews

In 2005, Huang and coworker synthesized triarylamine derivatives with siloxane groups to improve the performance of hole transporting in OLEDs [30]. The results show that siloxane groups can increase hole transporting performance with maximum luminance is about 64,000 cd/m^2 with turn-on voltage 4.0 V and quantum efficiency 2.4%.
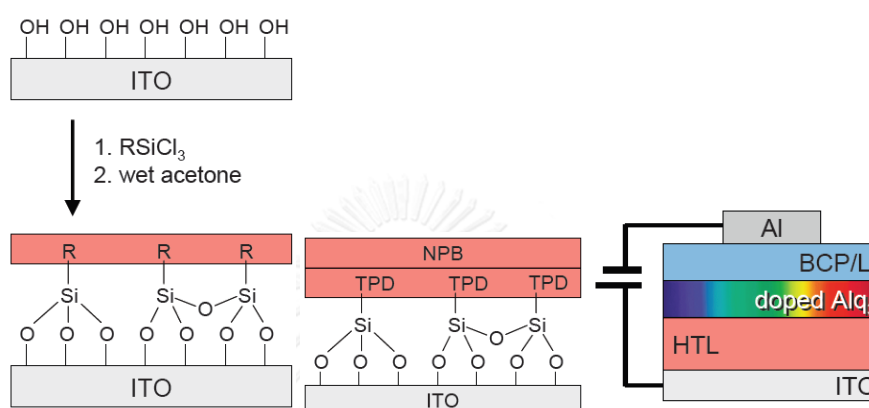
Figure 1.11 Chemical structures of triarylamine derivatives with siloxane groups and their OLED devices

In 2007, Lee and coworker have designed and synthesized 4,4′-bis-(3,5-bis-(diphenylamino)-phenyl)-1,1′-binaphthyl (PPBN), a derivative of triarylamine [31]. Its glass transition temperature (T$_g$) and decomposition temperature (T$_d$) were increased to 148 and 480 °C, respectively. In addition, PPBN played the role as hole transporting layer (HTL) instead of commercial hole transporting material, 4,4',4"-tris(2-naphthylphenylamino) triphenylamine (2-TNATA) to combination with tris(8-hydroxyquinoline) aluminium (Alq$_3$) was a function of EML. Its efficiency was enhanced to 80% when compared with the combination of 2-TNATA with Alq$_3$.
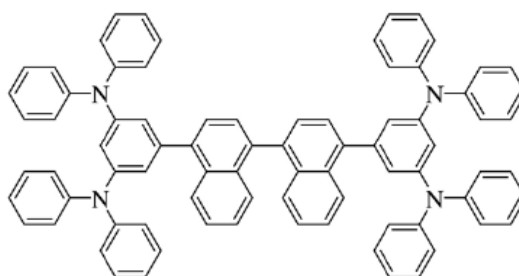
Figure 1.12 Chemical structures of PPBN

In 2007, Promarak and coworker studied the derivatives of carbazole [32]. G2CF was synthesized by using bromination and Ullmann coupling. It showed high glass transition temperature at 237 $^{\circ}$C and reversed electrochemical properties. To investigate the hole transporting properties, the OLED with structures of ITO/G2CF/Alq$_3$/LiF:Al were fabricated. The device with G2CF as an HTL shown maximum luminance in green light is about 11,000 cd/m^2 at 16 V with a turn on voltage of 5.4 V.
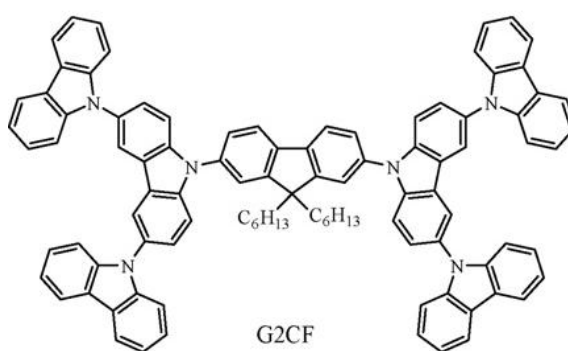
Figure 1.13 Chemical structures of G2CF

In 2012, Ruksasorn and coworker were designed and synthesized two derivatives of carbazole with truxene as a core structure (**Figure 1.14**) [33]. All compounds showed high glass transition temperatures at 249 and 293 °C, respectively. The decomposition temperature are at 392 and 371 ° C, respectively. Moreover, when used thses to form a thin film, the absorption were showed at wavelengths of 315 and 333 nm, respectively and the emission at wavelengths of 379 and 418 nm, respectively. However, two compounds have a quantum efficiency is not good.
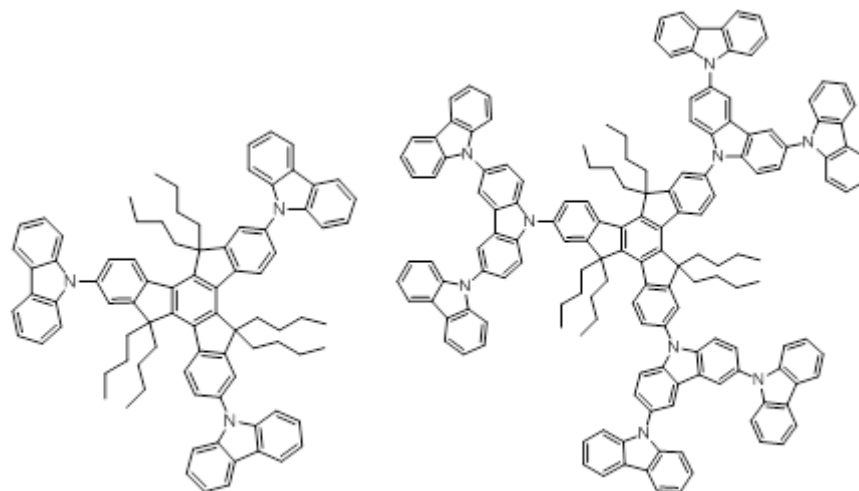
Figure 1.14 Two derivatives of carbazole with truxene as a core structure

In 2006, Feng and coworker synthesized derivatives of carbazole by using triazatruxene as a core structure [34]. T1 and T2 were studied and found that the optical properties, the absorption wavelength at 240, 295, 350 nm, and 248, 299, 350 nm, respectively. The emission in the blue region wavelength at 422 and 428 nm in the solution state and solid state, respectively.
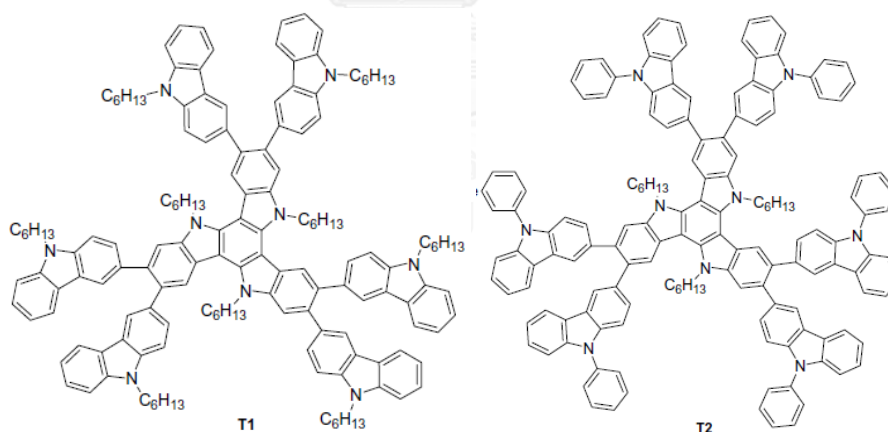
Figure 1.15 Chemical structures of T1 and T2

In 2006, Lai and coworker have synthesized derivatives of triazatruxene by using Suzuki coupling *via* microwave to obtained compounds T1-T3 [35]. When used it to study the optical properties, three compounds emit in the blue light at wavelength 429 and 440 nm, respectively. Then, T3 was investigated in OLED device in the structure of ITO / PEDOT: PSS / T3 / Ba / Al. Measurement electroluminescent found that the light emission at 442 nm.
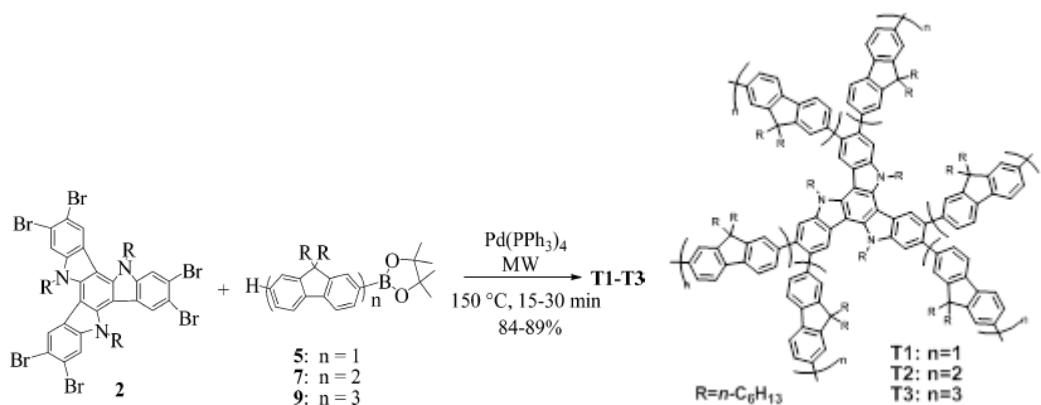
Figure 1.16 Synthesis and chemical structures of T1, T2 and T3

In 2012, Zhu and coworker synthesized triazatruxene derivatives with substituent at 3, 8, 13 positions in five categories [36]. Thermal properties of those compounds were investigated. Their T_d and T_m showed temperature measurement at 405 and 219-373, respectively. However, T_g could not observed for those compounds. Then, the exploration of optical properties was studied. They emitted blue light at 394-412 in solution and 416-461 in solid state, respectively. In addition, their quantum efficiency about 32-58%.
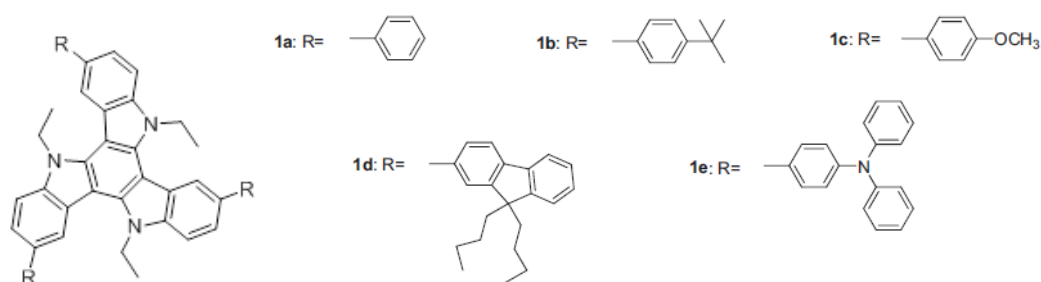
Figure 1.17 Chemical structures of triazatruxene derivatives with substituent at 3, 8, 13 positions

From the literature reviews, carbazole derivatives are well-known hole-transporting units because of their electron-donating capabilities associated with the nitrogen atom. From this reason, they were used as important building blocks for OLED materials. One of the electron-rich carbazole derivatives, 10, 15-dihydro-5H-dihydro-5H-diindolo [3,2-a:3',2'-c]carbazole or triindole, has become a famous

compound. Moreover, in my research group, truxene derivatives were designed and synthesized. The results showed that those compounds can be electroluminescence in blue light. Therefore, in this research, the series of novel star-shaped 3,8,13-substituted triindoles (TAT1 and TAT2) were investigated for hole transporting, high thermal stability and blue light-emitting layer as well.

In summary, the objectives of this work are following:

1. To synthesize compounds with triazatruxene derivatives for organic light-emitting diodes both emissive and hole-transporting materials.

2. To characterize and study the electronic, photophysical, electrochemical and thermal properties of the target molecules.

3. To investigate their potential application both emissive and hole-transporting materials for OLED.
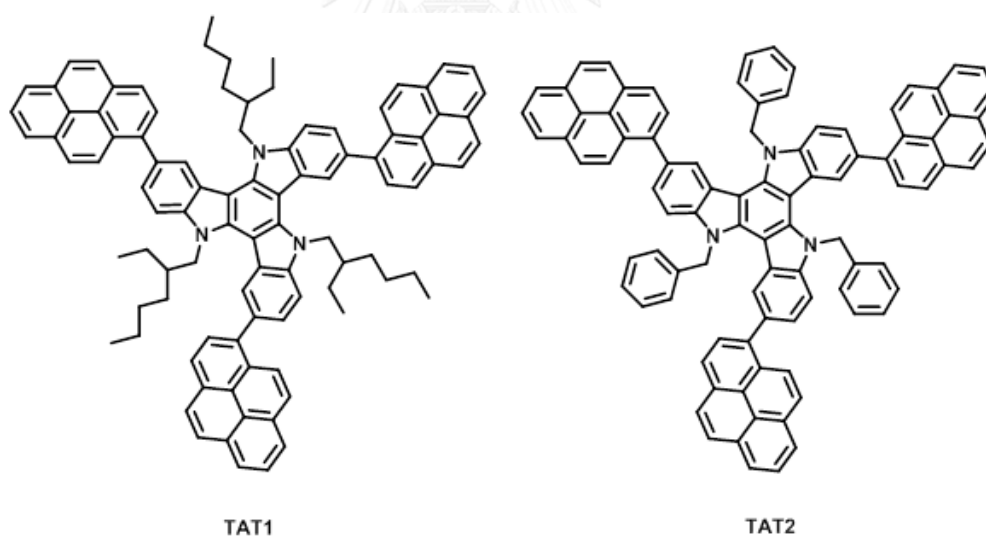
Figure 1.18 Chemical structure of target molecules (TAT1 and TAT2)

CHAPTER II

EXPERIMENTAL

2.1 Synthesis

2.1.1 Instruments and Equipment

Thin layer chromatography (TLC) was performed on aluminium sheets precoated with silica gel (Merck Kiesegel 60 F_{254}) (Merck KgaA, Darmstadt, Germany). Column chromatography was performed on silica gel (Merck Kieselgel 60G) (Merck KGaA, Darmstadt, Germany). All ^{1}H- and ^{13}C-NMR spectra were obtained on a Varian Mercury NMR spectrometer, which operated at 400 MHz for ^{1}H and 100 MHz for ^{13}C nuclei (Varian Company, CA, USA). Mass spectra were recorded on a Microflex MALDI-TOF mass spectrometer (Bruker Daltonics) using doubly recrystallized α-cyano-4-hydroxy cinnamic acid (CCA) and dithranol as a matrix. Absorption spectra were measured by a Varian Cary 50 UV-Vis spectrophotometer. Fluorescence spectra were obtained from a Varian Cary Eclipse spectrofluorometer.

The fluorescence quantum yields (Φ) were determined by comparison with a standard of known fluorescence quantum yield according to the following equation [37].

$$\Phi_{X=} \Phi_{ST}\left(\frac{Slope_X}{Slope_{ST}}\right)\left(\frac{\eta_X^2}{\eta_{ST}^2}\right)$$

Where the subscripts X refer to the unknown samples and ST refers to the standard quinine sulfate solution in 0.01 M H_2SO_4, whose fluorescence quantum yield is known to be 0.54 , Φ is the fluorescence quantum yield, *Slope* is the slope from the plot of integrated fluorescence intensity versus absorbance, and η is the refractive index of the solvent. The refractive indexes of CH_2Cl_2 and 0.01 M H_2SO_4 were 1.424 and 1.333, respectively.

The electrochemical analysis by cyclic voltametry was performed using an AUTOLAB spectrometer. All measurements were made at room temperature on sample solutions in freshly distilled dichloromethane with 0.1 M tetra-n-butylammonium hexafluorophosphate as electrolyte. Dichloromethane was distilled from calcium hydride and the electrolyte solutions were degassed by nitrogen bubbling. A glassy carbon working electrode, a platinum wire counter electrode, and a Ag/AgNO$_3$ (Sat.) reference electrode were used in all cyclic voltametric experiments.

Thermal experiments with Differential Scanning Calorimeter (DSC) were performed on Mettler Toledo DSC 822^e and Thermogravimetric Analysis (TGA) were studied using Simultaneous Thermal Analyzer Netzsch 409.

2.1.2 Synthetic procedures

10,15-Dihydro-5H-dihydro-5H-diindolo[3,2-a:3',2'-c]carbazole (3):

A mixture of indole (2 g, 17 mmol) and CH$_3$CN (5 mL) was stirred at room temperature and solution of Br$_2$ (1.3 mL, 51 mmol) in CH$_3$CN (15 mL) was added over 5 min. The mixture was stirred overnight, and the resulting dark-green solid was filtered and washed with acetonitrile (250 mL). At this point, without further purification, the crude product (3 g) was mixed with Et$_3$N (8.4 mL, 60.46 mmol), HCOOH (2.28 mL, 60.46 mmol) and 10% Pd/C (400 mg, 0.36 mmol) in MeOH (50 mL), and the resulting mixture was heated for 30 min under reflux. The mixture was filtered through Celite, and the filtrate was diluted with CH$_2$Cl$_2$, washed with aqueous HCl (10%) and dried (Na$_2$SO$_4$), and the solvent was evaporated under reduced pressure to give brown solid (2 g). The crude product was dissolved in methanol, adsorbed onto silica gel and purified by chromatography (ethyl acetate/n-hexane, 15:85) to give pure **3** as a pale-yellow solid (0.16 g, 16%). ^{1}H-NMR (400 MHz, acetone) δ 11.16 (s, 3H), 8.57 (d, J = 7.5 Hz, 3H), 7.74 (d, J = 7.8 Hz, 3H), 7.35 (dt, J = 22.8, 7.2 Hz, 6H). The ^{1}H-NMR spectrum is in good agreement with the literature report [38].

3,8,13-Tribromo-10,15-dihydro-5H-diindolo [3,2-a:3',2'-c]carbazole (4):

A solution of N-bromosuccinimide (NBS) (0.28 g, 1.55 mmol) in dimethylformamide (2 mL) was added dropwise to a mixture of **3** (0.17 g, 0.5 mmol) in acetone (10 mL) at 0 °C. The mixture was slowly warmed to room temperature and stirred for an additional 30 min before it was poured into water. Then, the organic phase was separated and dried over anhydrous Na_2SO_4. After the solvent was evaporated, the crude product was purified by column chromatography using hexane/acetone (8:2) as the eluent to afford **4** as a pale white solid (0.22 g, 76%). ^{1}H NMR (400 MHz, acetone) δ 11.34 (s, 3H), 8.39 (d, J = 8.3 Hz, 3H), 7.85 (s, 3H), 7.45 (d, J = 6.8 Hz, 3H).

5,10,15-Triethylhexyl-10,15-dihydro-5H-diindolo[3,2-a:3',2'-c]carbazole (5):

A mixture of **4** (0.15 g, 0.25 mmol) and KOH (0.28 g, 5 mmol) was stirred at room temperature, then a solution of ethylhexylbromide (0.27 mL, 1.5 mmol) was added slowly, the mixture was stirred overnight. The mixture was poured into water and extracted with EtOAc. The combined organic layer was dried over anhydrous Na_2SO_4, filtered, and concentrated under reduce pressure., the crude product was purified by chromatography (EtOAc:n-hexane, 5:95) to give the compound **5** as a yellow solid (0.22 g, 95%). ^{1}H NMR (400 MHz, CDCl$_3$) δ 7.86 (d, J = 8.5 Hz, 3H), 7.52 (s, 3H), 7.46 (d, J = 8.6 Hz, 3H), 4.40 (s, 6H), 1.79 (s, 3H), 1.10 – 0.44 (m, 42H).

5,10,15-Tribenzyl-10,15-dihydro-5H-diindolo[3,2-a:3',2'-c]carbazole (6):

A mixture of **4** (0.15 g, 0.25 mmol), KOH (0.28 g, 5 mmol), and $[CH_3(CH_2)_3]_4N(HSO_4)$ (0.0083 g, 0.025 mmol) was heated to reflux in acetone (10 mL). Benzyl bromide (0.2 mL, 1.68 mmol) was then added and the mixture was stirred for 3 h. The mixture was diluted with CH_2Cl_2, washed with 10% aqueous HCl

and with saturated aqueous NaCl solution, and dried (Na$_2$SO$_4$), the solvent was then evaporated. The residue was triturated with hexanes to give **6** as a white solid (0.21 g, 98%). ^{1}H NMR (400 MHz, CDCl$_3$) δ 8.12 (s, 3H), 7.89 (d, J = 7.0 Hz, 3H), 7.74 (d, J = 8.5 Hz, 3H), 7.47 (m, 9H), 7.10 (d, J = 7.2 Hz, 6H), 5.96 (s, 6H).

5,10,15-Triethylhexyl-3,8,13-tri(pyren-1-yl)-10,15-dihydro-5H-diindolo[3,2-a:3',2'-c]carbazole (TAT1):

To a degassed (N$_2$) solution of **5** (0.09 g, 0.1 mmol) and Pd(PPh$_3$)$_4$ catalyst (0.012 g, 0.01 mmol) in toluene (5 mL), then pyreneboronic acid (0.1476 g, 0.6 mmol) and 2 M aqueous K$_2$CO$_3$ solution (1 mL) were added via syringe. The reaction mixture was stirred at 70 ^{o}C for 48 h. After cooling, the product was extracted with CH$_2$Cl$_2$, washed with water, and dried over anhydrous Na$_2$SO$_4$. The solvent was evaporated, affording the crude mixture. The crude product was purified by column chromatography (CH$_2$Cl$_2$:n-hexane, 1:9) to give the compound **TAT1** as a yellow solid (83.1 mg, 65%). ^{1}H NMR (400 MHz, CDCl$_3$) δ 8.47 (d, J = 9.2 Hz, 3H), 8.35 − 7.88 (m, 30H), 7.67 (s, 3H), 5.09 (s, 6H), 2.28 (d, J = 12.1 Hz, 3H), 1.70 (s, 6H), 1.41 (s, 3H), 1.20 − 0.55 (m, 39H). ^{13}C NMR (100 MHz, CDCl$_3$) δ 150.2, 141.6, 136.5, 131.8, 131.31, 131.25, 130.6, 129.8, 129.1, 129.0, 128.3, 127.7, 127.6, 127.5, 126.5, 126.2, 126.0, 125.34, 125.25, 124.9, 124.8, 122.7, 122.2, 113.8, 51.1, 38.6, 34.5, 33.9, 28.5, 23.3, 14.0, 10.6. MALDI-TOF MS (*m/z*): calcd: (1282.693 [C$_{96}$H$_{87}$N$_3$]); found: (1281.797 [M$^+$]).

5,10,15-Tribenzyl-3,8,13-tri(pyren-1-yl)-10,15-dihydro-5H-diindolo[3,2-a:3',2'-c]carbazole (TAT2):

To a degassed (N$_2$) solution of **6** (85.2 mg, 0.1 mmol) and Pd(PPh$_3$)$_4$ catalyst (11.6 mg, 0.01 mmol) in toluene (5 mL), then pyreneboronic acid (14.8 mg, 0.6 mmol) and 2 M aqueous K$_2$CO$_3$ solution (1 mL) were added via syringe. The reaction mixture was stirred at 70 ^{o}C for 48 h. After cooling, the product was extracted with CH$_2$Cl$_2$, washed with water, and dried over anhydrous Na$_2$SO$_4$. The solvent was evaporated, affording the crude mixture. The crude product was purified by column chromatography (CH$_2$Cl$_2$:n-hexane, 2:8) to give the compound **TAT2** as a

yellow solid (0.06 g, 49%). ^{1}H NMR (400 MHz, CDCl$_3$) δ 8.12 (d, J = 7.9 Hz, 3H), 7.90 (m, 30H), 7.70 (d, J = 9.2 Hz, 3H), 7.47 (s, 3H), 7.38 (d, J = 6.6 Hz, 6H), 7.28 (d, J = 7.2 Hz, 6H), 6.04 (s, 6H). ^{13}C NMR (100 MHz, CDCl$_3$) δ 141.8, 140.3, 138.2, 138.1, 136.4, 131.6, 131.1, 130.4, 129.3, 128.6, 128.1, 127.7, 127.5, 127.4, 127.3, 126.8, 126.0, 125.5, 125.02, 124.98, 124.7, 124.6, 123.4, 122.5, 121.7, 113.2, 103.5, 51.5. MALDI-TOF MS (m/z): calcd: (1216.459 [C$_{93}$H$_{57}$N$_3$]); found: (1215.485 [M$^+$]).

2.2 OLED device fabrication section

2.2.1 Commercially available materials

The commercial sources and purities of materials used in these experiments are shown in **Table 2.1**. All materials were analytical grade and used without further purification, unless indicated.

Table 2.1 Commercially available materials for OLED device fabrication.

Materials	Purity (%)	Company
1″ × 1″ Indium oxide doped tin oxide (99.3 wt % In$_2$O$_3$:0.7 wt % SnO$_2$)-coated glasses (5-15 ohm/sq)	99.5	Kintec
Poly(3,4-ethylenedioxythiophene)–poly(styrene) (0.5 wt % PEDOT: 0.5 wt % PSS)	1.3	Baytron
Tris(8-hydroxyl-quinoline) aluminum (Alq$_3$)	98	Sigma-Aldrich
Lithium fluoride (LiF)	99.98	ACROS
Aluminium (Al) wire	99.97	BDH
2,9-dimethyl-4,7-diphenyl-1,10-phenanthroline (BCP)	99	Sigma-Aldrich
N,N-diphenyl-N,N'-bis(1-naphthyl)-(1,1'-biphenyl)-4,4'- diamine (NPB)	99	Sigma-Aldrich

2.2.2 Reagents

The reagents were obtained from various suppliers as shown in **Table 2.2**. All reagents were analytical grade and used without further purification, unless indicated.

Table 2.2 List of reagents

Reagents	Purity (%)	Company
Hydrochloric acid (HCl) 37%	36.5	Carlo Erba
Nitric acid (HNO$_3$) 69%	68.5-69.5	BDH
Sodium hydroxide (NaOH)	99.99	Carlo Erba
Acetone	99.5	BDH
Isopropanol	99.5	Carlo Erba

2.2.3 Instruments

The following instruments were used in this study:

(1) Photoluminescence (PL) spectrophotometer (Perkin–Elmer, Model LS 50B)

(2) Spin-coater (Chemat Technology, Model KW-4A)

(3) Thermal evaporator (ANS Technology, Model ES280)

(4) Digital source meter (Keithley, Model 2400)

(5) Multifunction optical meter (Newport, Model 1835-C)

(6) Calibrated photodiode (Newport, Model 818 UVCM)

(7) USB Spectrofluorometer (Ocean Optics, Model USB4000FL)

2.2.4 Organic thin film preparation and characterization

The preparation process of organic thin films is described in **Figure 2.1**.
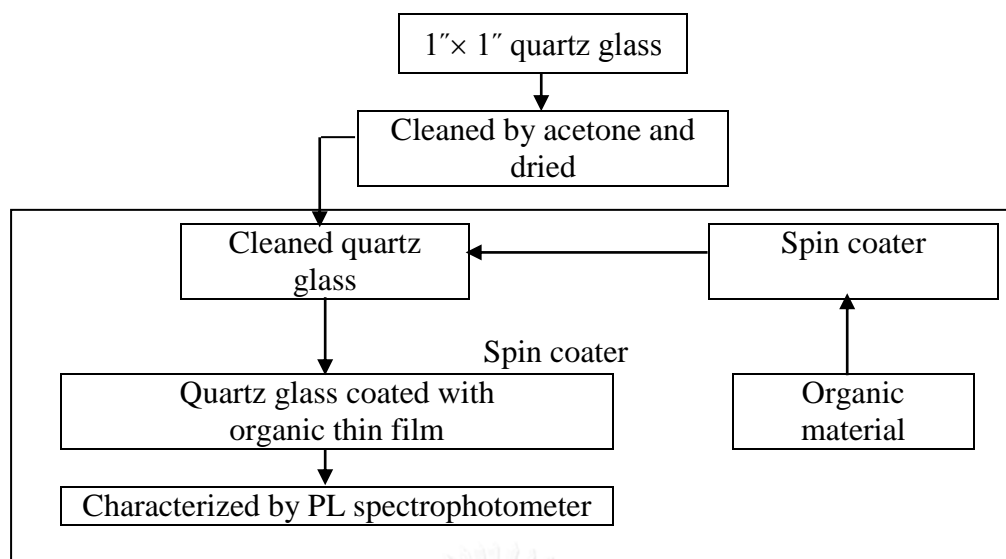
Figure 2.1 Preparation and characterization of organic thin film

2.2.5 Spin coating technique of organic thin film

In order to study the photo physical properties of solid-state materials, organic thin films coating on quartz glass substrates (1″x1″) were prepared by spin coater. Prior to film deposition, the substrates were cleaned with acetone in ultrasonic bath followed by drying on a hotplate. The organic material was dissolved in the solution of CH_2Cl_2 : toluene (2:1 %v/v) and then filtered through a 0.45 µm pore size nylon filter (Orange scientific) and spin-coated onto a cleaned quartz glass surface at 2000 rpm for 20 sec. Finally, the quartz glass coated with the organic film was baked at 100 ^{o}C for 10 min.

2.2.6 OLED device fabrication

The OLEDs fabrication process is described in **Figure 2.2a** and **Figure 2.2b**.

```
┌─────────────────────────────────────┐
│      1″× 1″ ITO-coated glasses       │
└─────────────────────────────────────┘
                  │
                  ▼
┌──────────────────────────────────────────────────────────────────┐
│  Etched with HCl : HNO₃ = 1 : 3 (v/v) (aqua regia) to give        │
│  patterned ITO glasses                                             │
└──────────────────────────────────────────────────────────────────┘
                  │  Cleaned and dried
                  ▼
         ┌─────────────────────────────────┐
         │  Fresh patterned ITO glass (G)  │
         └─────────────────────────────────┘
                  │
┌──────────────────────┐          │
│ PEDOT:PSS solution   │ ───────► "Spin coated"
└──────────────────────┘          │
                                  ▼
         ┌─────────────────────────────────────┐
         │  G coated with PEDOT:PSS film (GP)   │
         └─────────────────────────────────────┘
                  │
┌──────────────────────┐          │
│    TAT1 or TAT2      │ ───────► "Spin coated"
└──────────────────────┘          │
                                  ▼
         ┌─────────────────────────────────────┐
         │  GP coated with TAT1 or TAT2 (GPT)   │
         └─────────────────────────────────────┘
                  │
┌──────────────────────┐          │
│        Alq₃          │ ───────► "Thermal evaporated"
└──────────────────────┘          │
                                  ▼
         ┌─────────────────────────────────────┐
         │    GPT coated with Alq₃ (GPTQ)       │
         └─────────────────────────────────────┘
                  │
┌──────────────────────┐          │
│       LiF/Al         │ ───────► "Thermal evaporated"
└──────────────────────┘          │
                                  ▼
         ┌─────────────────────────────────────┐
         │             OLED (A)                │
         └─────────────────────────────────────┘
                  │
                  ▼
         ┌─────────────────────────────────────┐
         │      Performance measurement        │
         └─────────────────────────────────────┘
```
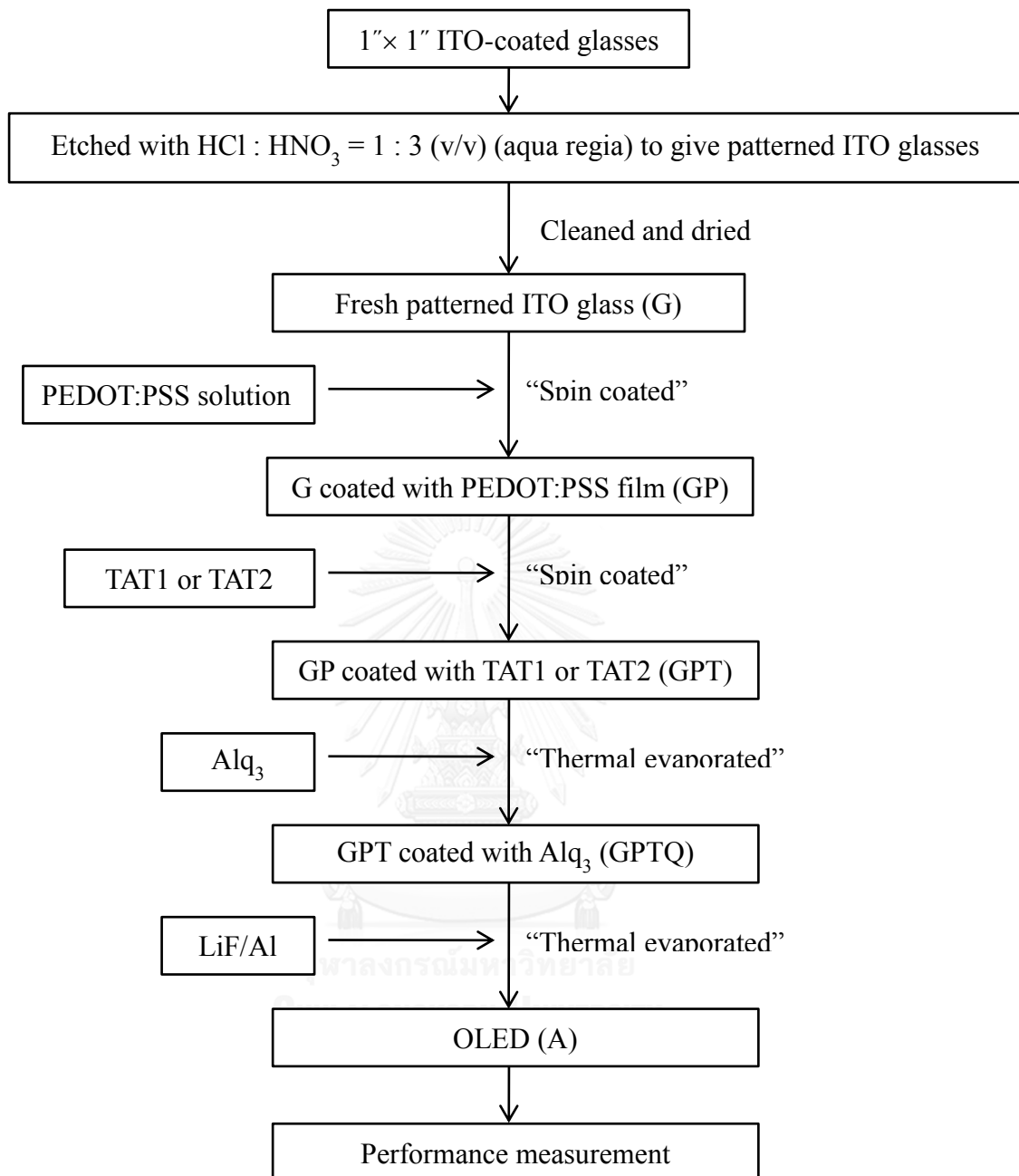
Figure 2.2a Fabrication and measurement of OLED for study HTL

```
┌─────────────────────────────────┐
│    1″× 1″ ITO-coated glasses     │
└─────────────────────────────────┘
                 │
                 ▼
┌───────────────────────────────────────────────────────────────────┐
│ Etched with HCl : HNO₃ = 1 : 3 (v/v) (aqua regia) to give patterned ITO glasses │
└───────────────────────────────────────────────────────────────────┘
                 │  Cleaned and dried
                 ▼
┌─────────────────────────────────┐
│   Fresh patterned ITO glass (G)  │
└─────────────────────────────────┘

┌──────────────────────┐
│ PEDOT:PSS solution   │ ────────▶  "Spin coated"
└──────────────────────┘
                 │
                 ▼
┌─────────────────────────────────┐
│ G coated with PEDOT:PSS film (GP)│
└─────────────────────────────────┘

┌──────────────────────┐
│   TAT1 or TAT2       │ ────────▶  "Spin coated"
└──────────────────────┘
                 │
                 ▼
┌─────────────────────────────────┐
│ GP coated with TAT1 or TAT2 (GPT)│
└─────────────────────────────────┘

┌──────────────────────┐
│        BCP           │ ────────▶  "Thermal evaporated"
└──────────────────────┘
                 │
                 ▼
┌─────────────────────────────────┐
│   GPT coated with BCP (GPTB)     │
└─────────────────────────────────┘

┌──────────────────────┐
│       LiF/Al         │ ────────▶  "Thermal evaporated"
└──────────────────────┘
                 │
                 ▼
┌─────────────────────────────────┐
│            OLED (B)              │
└─────────────────────────────────┘
                 │
                 ▼
┌─────────────────────────────────┐
│     Performance measurement      │
└─────────────────────────────────┘
```

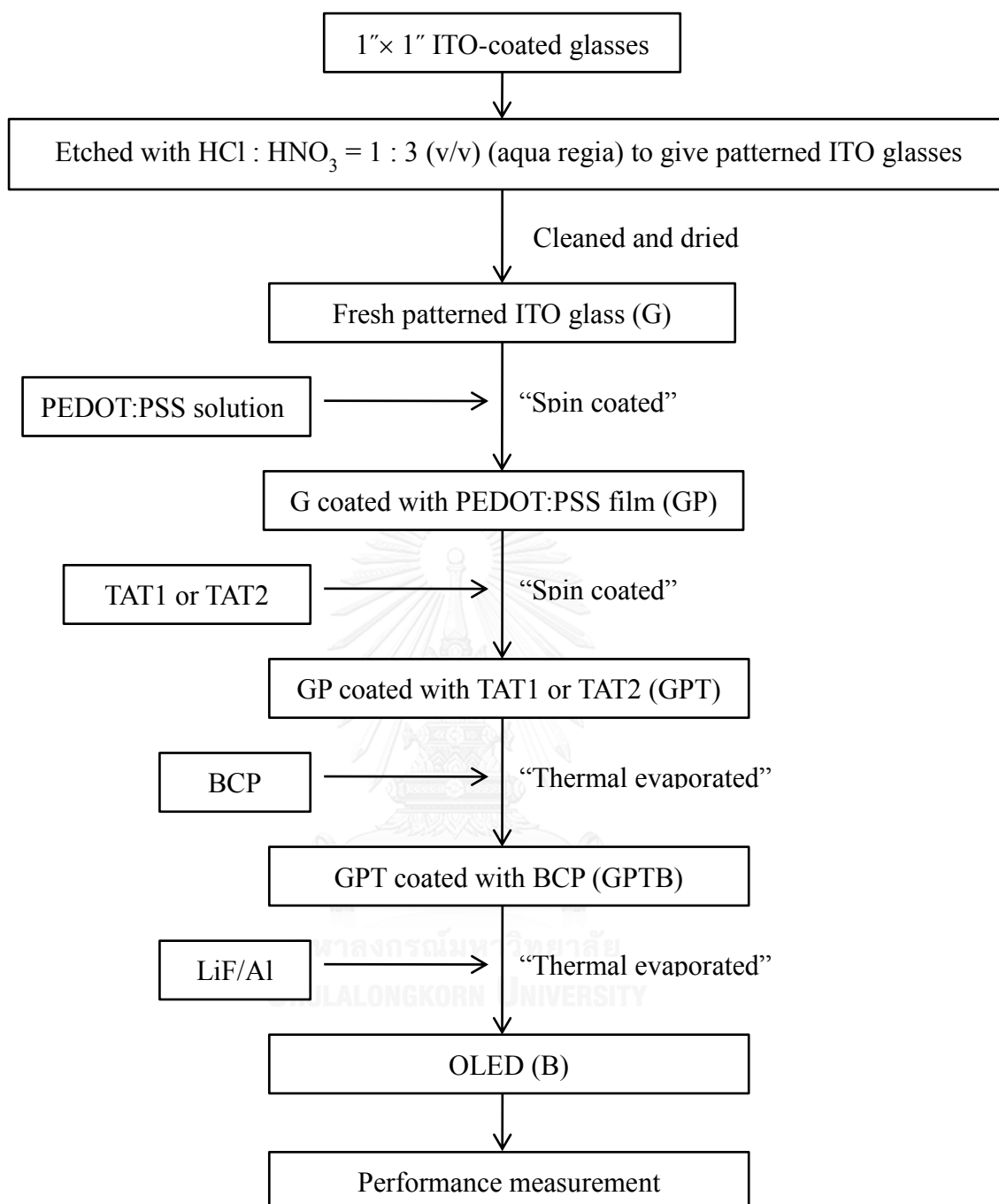**Figure 2.2b** Fabrication and measurement of OLED for study EML

2.2.7 Patterning process for ITO-coated glasses

The ITO-coated glasses **Figure 2.3(a)** were firstly etched to give a pattern of ITO sheet on glass. Prior to the patterning process, the ITO sheet on glass was covered with a 2 x 10 mm of negative dry film photo resist (Warf) [39]. The covered ITO glass **Figure 2.3(b)** was immersed in the solution of HCl:HNO$_3$ (1:3 v/v) (aqua regia) for 10 min, with stirring during the etching process. The etched ITO glass was cleaned by thoroughly rinsing with water and subsequently soaking in 0.5 M NaOH for 10 min to remove the negative dry film from an ITO-coated glass surface. Finally, these substrates were thoroughly rinsed with water to give the patterned ITO glasses as shown in **Figure 2.3(c)**.
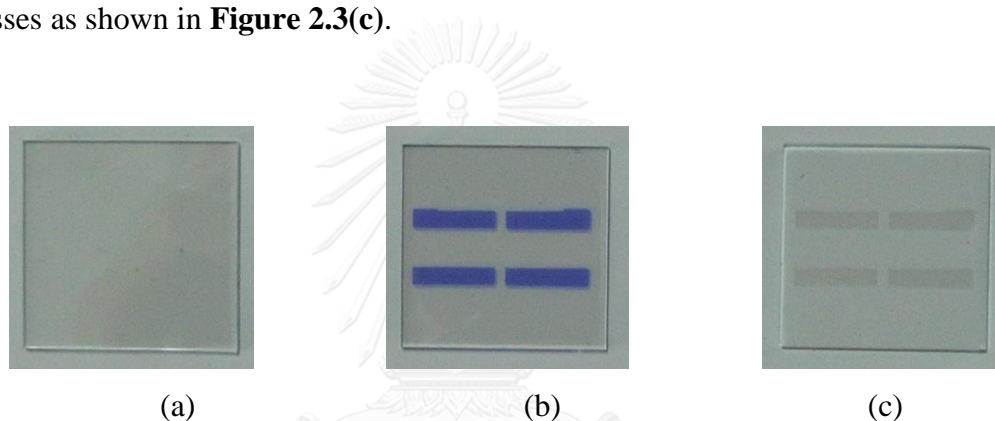

(a)   (b)   (c)

Figure 2.3 (a) ITO-coated glass, (b) ITO-coated glass covered with 2 x 10 mm of negative dry film photo resist and (c) patterned ITO glass

2.2.8 Cleaning process for the patterned ITO glasses

The cleanliness of the ITO surface was an important factor in the performance of the OLEDs devices. The patterned ITO glasses were cleaned for 10 min with detergent in ultrasonic bath followed by a thorough rinse with de-ionized (DI) water and then subsequently ultra-sonicated in hot acetone and isopropanol for 10 min. Finally, the substrates were dried in vacuum oven at 100 °C to give fresh patterned ITO glasses.

2.2.9 Spin-coating method of PEDOT:PSS

A PEDOT:PSS solution was diluted with isopropanol and stirred for 1 day. The spin-coating method was performed on a spin coater as shown in **Figure 2.4**. The diluted PEDOT:PSS solution was filtered through a 0.45 µm pore size nylon

filter (Orange scientific) and spin-coated onto a fresh patterned ITO glass surface at 2000 rpm for 20 sec. Finally, the patterned ITO glass coated with the PEDOT:PSS film was baked at 100 °C for 10 min for curing.
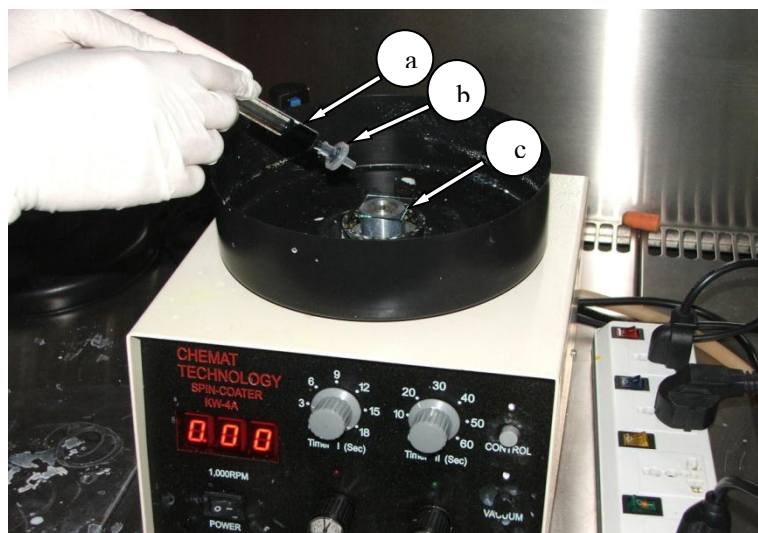

Figure 2.4 Spin-coating method by using a spin coater. (a) PEDOT:PSS solution in the syringe, (b) nylon filter, and (c) fresh patterned ITO glass

2.2.10 Organic thin film deposition

The deposition of other organic layers was the next step in the fabrication of OLEDs. The organic layers were deposited using spin coating (**Figure 2.4**) with the same procedure described in section 2.2.5. Prior to the deposition, the patterned ITO glass coated with PEDOT:PSS film or/and the fresh patterned ITO glass were placed on a substrate holder. The organic materials was dissolved in the solution of $CHCl_3$:toluene (2:1 v/v) and then filtered through a 0.45 µm pore size nylon filter (Orange scientific) and spin-coated onto a patterned ITO glass coated with PEDOT:PSS film surface at 2000 rpm for 20 sec. Finally, the ITO glass coated with the organic film was baked at 100 °C for 10 min. In addition, for OLED(A) (**Figure 2.3a**), the organic materials, such as Alq_3, were loaded in co-evaporation sources, alumina filament boat 1 and 2, respectively, into a vacuum chamber of the thermal evaporator. These organic materials were deposited on top of glass substrates

by co-evaporation of the two source materials at a background pressure of approximately 1×10^{-5} mbar with $0.2 - 0.4$ Å/sec evaporation rate.

2.2.11 Hole blocking and cathode deposition

After organic thin film deposition by the technique of spin coating, the next step is increasing hole blocking layer before closing with cathode deposition (**Figure 2.3b**). 2,9-dimethyl-4,7-diphenyl-1,10-phenanthroline (BCP) was evaporated from tungsten boat to deposit at the device. Finally, an ultra thin LiF layer and Al cathode contact were sequentially co-evaporated from two tungsten boats through a shadow mask (**Figure 2.5**) with 2 mm wide slits arranged perpendicularly to the ITO fingers, to obtain the OLED with an active area of 2×2 mm^2 (**Figure 2.6**). The operating vacuum for evaporation of this cathode was under 1×10^{-5} mbar at high evaporation rates of $5 - 10$ Å/sec. The thickness of LiF and Al of all devices were 0.5 and 150 nm, respectively.
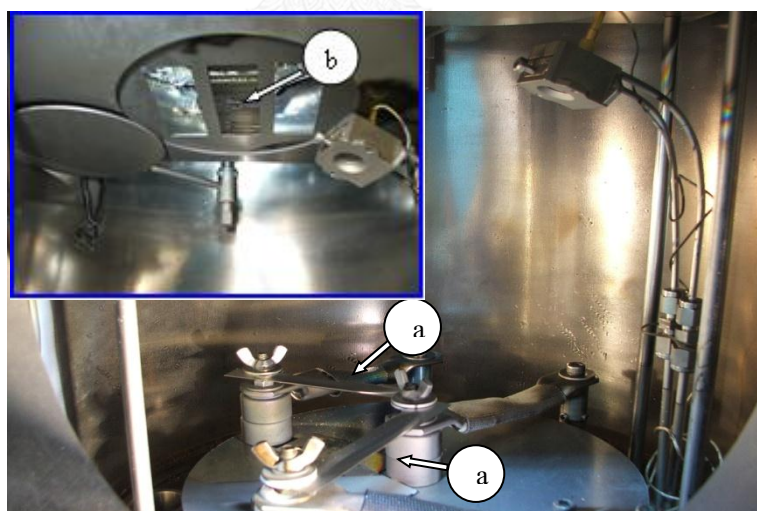

Figure 2.5 Instrument for cathode deposition. (a) tungsten boats and (b) 2 mm wide fingers of a shadow mask
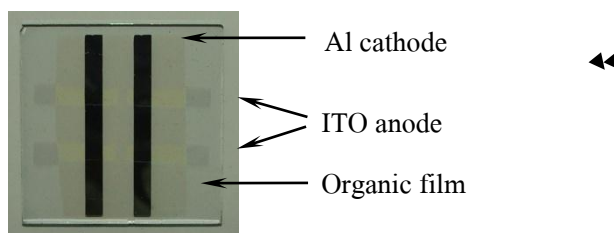
Al cathode

ITO anode

Organic film

Figure 2.6 shows the OLED device fabricated by thermal evaporation with 4 pixels. A pixel active area of a device is 2×2 mm^2.

2.2.12 Device measurement

The instruments for OLED device measurements are shown in **Figure 2.7**. The computer was used for controlling of the digital source meter, the multifunction optical meter, and the USB spectrofluorometer as well as recording the data. The digital source meter applied the voltages to the device and measured the resulting currents. The multifunction optical meter connected with the calibrated photodiode served in the measurement of the luminance (brightness). The USB spectrofluorometer was used for the EL spectra acquisition.
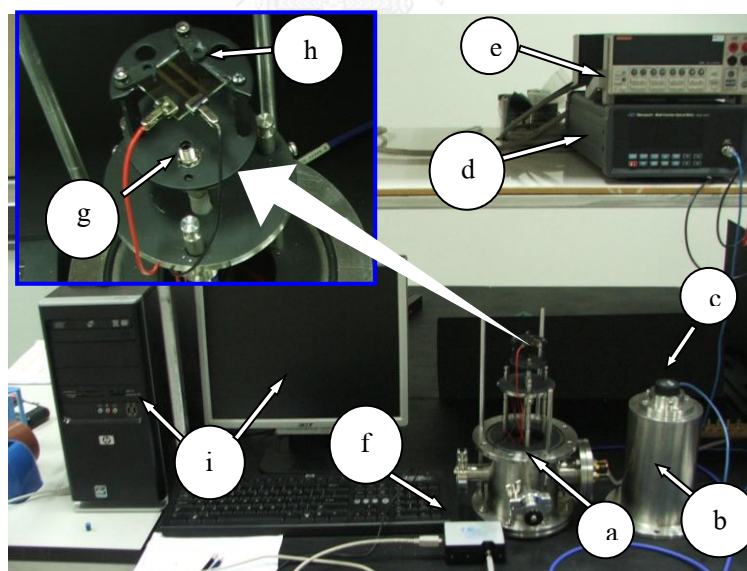

Figure 2.7 Instruments for determination of OLED device performance: (a) OLED test box, (b) lid of OLED test box, (c) calibrated photodiode, (d) multifunction optical meter, (e) digital source meter, (f) USB spectrofluorometer, (g) probe of USB spectrofluorometer, (h) OLED device holder, (i) computer controller and recorder for digital source meter, multifunction optical meter, and USB spectrofluorometer

All device measurements were performed in an OLED test box by blocking the incident light at room temperature under ambient atmosphere. When voltages were applied, the currents, brightness, and EL spectra were recorded at the same time to give the current density–voltage–luminance (*J-V-L*) characteristics and EL spectra. The turn-on voltage was defined at the brightness of 1 cd/m^2. The current density was calculated as the following formula (1):

$$J = \frac{I}{A} \tag{1}$$

Here, *I* (mA) is the current and *A* (cm^2) is the pixel active area of the device. The luminous efficiency of the device was calculated as the following formula (2):

$$\eta_{\text{lum}} = \frac{L}{J} \tag{2}$$

Here, *L* (cd/m^2) is the luminance and *J* (mA/cm^2) is the current density. The quantum efficiency of a device can be differentiated into two categories; internal and external quantum efficiencies.

Internal quantum efficiency (IQE)- This is the total number of photons generated inside the device per electron– hole pair injected into the device. It is represented by η_{int}. For OLEDs the internal quantum efficiency in the case of fluorescent materials is given by (OIDA 2002)

$$\eta_{\text{int}} = \gamma\,\eta_{\text{s}}\Phi_{\text{f}}, \tag{3}$$

where γ is the fraction of injected charges that produce excitons and is called the charge balance factor, η_{s} is the fraction of singlet excitons called singlet exciton efficiency and Φ_{f} is the fraction of energy released from material as light and called the quantum efficiency of fluorescence.

External quantum efficiency (EQE)- This is defined as the total number of photons emitted from the device per electron–hole pair injected into the device. It is represented by η_{ext}. The external quantum efficiency is related to the internal quantum efficiency and is given by (OIDA 2002)

$$\eta_{\text{ext}} = R_{\text{e}}\,\eta_{\text{int}}, \tag{4}$$

where R_e is the extraction or outcoupling efficiency representing the number of photons emitted from the device per number of photons generated in the device.

Power Efficiency

The luminous efficacy or power efficiency is the lumen output per input electrical power of the device. It is measured in lumen per watt (lm/W) or candela per ampere (cd/A). It is represented by η_p.

2.2.13 The coordinate value calculation of Commission Internationale de l'Eclairage 1931 (CIE 1931)

The coordinate value of CIE 1931 was calculated from the EL spectrum. In the study of the perception of color, one of the first mathematically defined color spaces was the CIE 1931 XYZ color space, created by the International Commission on Illumination (CIE) in 1931. The CIE XYZ color space was derived from a series of experiments done in the late 1920s by Wright [40] and Guild [41]. Their experimental results were combined into the specification of the CIE RGB color space, from which the CIE XYZ color space was derived. Firstly, the tristimulus value was calculated as the following formula (5):

$$X = 683 \int_{360}^{830} S(\lambda)\bar{x}(\lambda)\Delta(\lambda), \ Y = 683 \int_{360}^{830} S(\lambda)\bar{y}(\lambda)\Delta(\lambda), \ Z = 683 \int_{360}^{830} S(\lambda)\bar{z}(\lambda)\Delta(\lambda)$$

(5)

Here, $S(\lambda)$ is the spectral data; X, Y, and Z are the tristimulus values; and $\bar{x}$, $\bar{y}$, and $\bar{z}$ are the tristimulus functions.

The coordinate value of CIE 1931 was calculated from formula (6):

$$\text{CIE 1931 } x = \frac{X}{X+Y+Z} \ , \text{CIE 1931 } y = \frac{Y}{X+Y+Z} \tag{6}$$

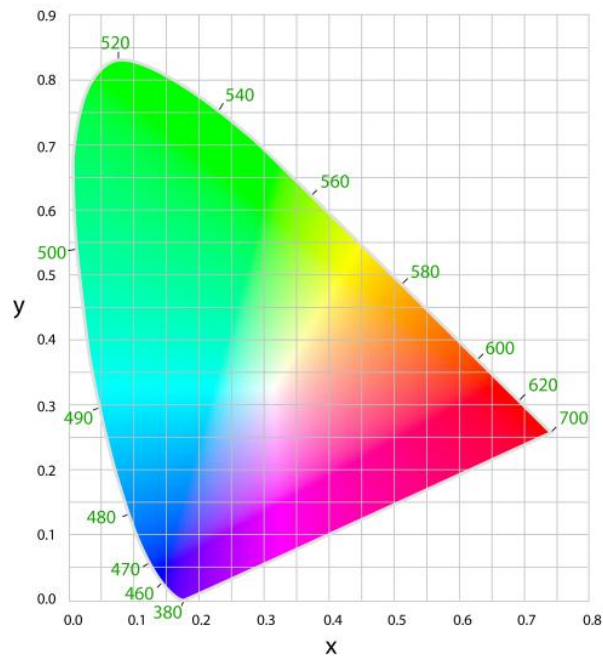The CIE 1931 chromaticity is shown in **Figure 2.8**.

Figure 2.8 CIE 1931 chromaticity

Note; the parameters used to evaporate all materials are the parameters of Al only, such as density of Al = 2.7. Thus, to evaluate the real thickness of the organic layers deposited by thermal evaporator and the thickness of PEDOT:PSS layer deposited by spin coating method, in the future, the glass substrate will be measured by scanning electron microscope (SEM) or/and the atomic force microscope (AFM). The real calculation of the CIE coordinate was obtained by the Microsoft office excel 2007 with the calculated formula of CIE 1931.

CHAPTER III
RESULTS AND DISCUSSION

3.1 Synthesis

Two triazatruxene derivatives (TAT1, TAT2) were synthesized from triazatruxene core and pyrene branch *via* Suzuki cross-coupling reaction. First, triazatruxene core was synthesized by bromine-catalyzed cyclotrimerization of indole to obtain mixture products of **2**. Then, it was used as a starting material in the next step without purification for reductive de-bromination by using Pd-catalyst and triethylammonium formate to give **3** (**Scheme 3.1a**). Alternatively, N-bromo succinamide (NBS) was used for bromine-catalyzed cyclotrimerization under the same condition with bromine (**Scheme 3.1b**). The structure of **3** was confirmed by ^{1}H-NMR which were in good agreement with the literature reports [38].
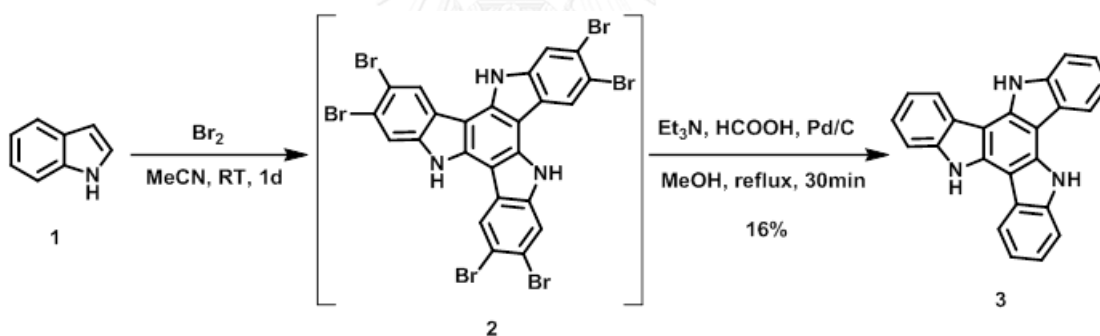
Scheme 3.1a The synthesis of triazatruxene core by bromination of indole with bromine
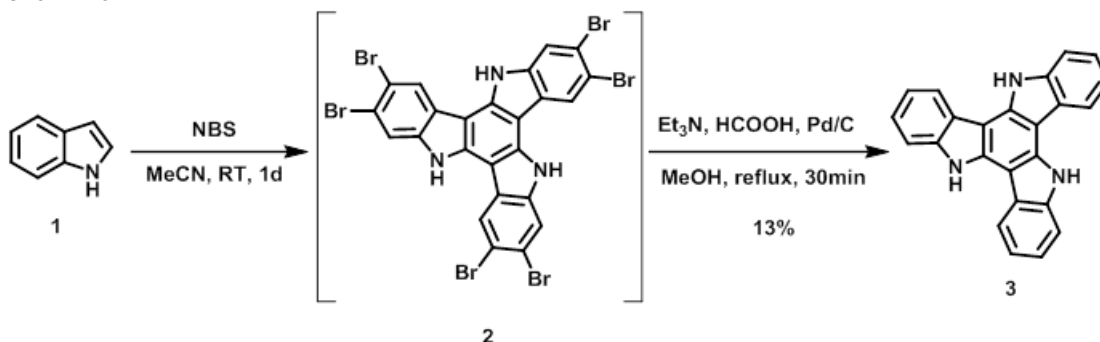
Scheme 3.1b The synthesis of triazatruxene core by bromination of indole with NBS
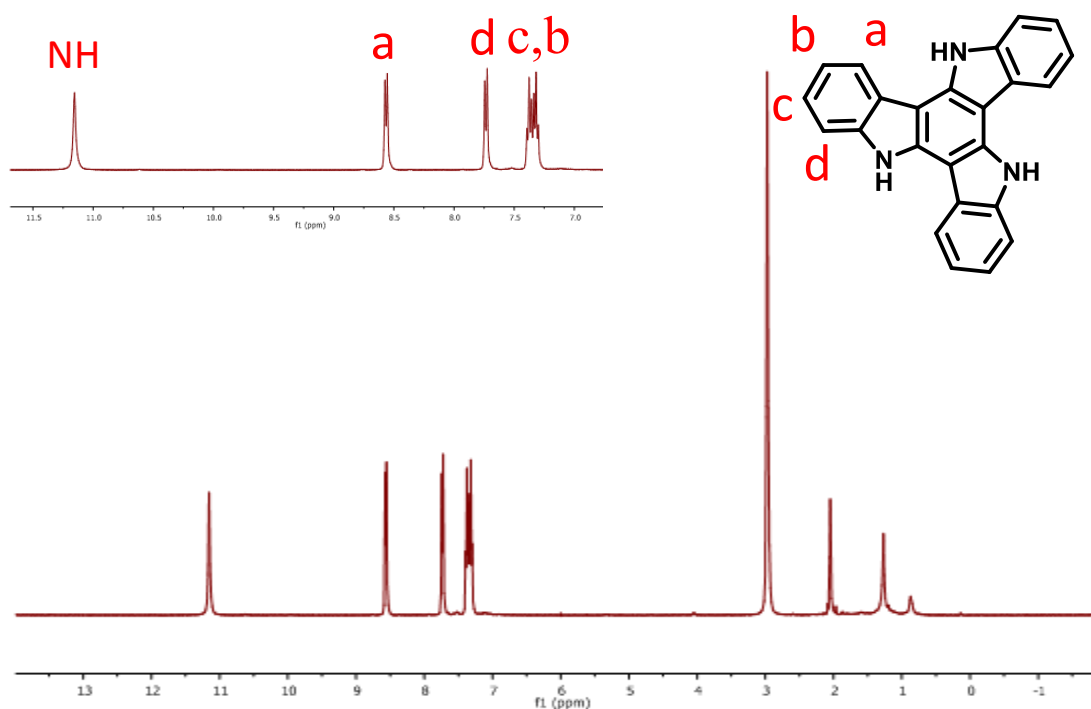
Figure 3.1 ^{1}H-NMR of triazatruxene core (**3**) in acetone-d6

In the reaction mechanism, indole was first brominated at the 3-position, then the bromoindoles can dimerize and trimerize by nucleophilic replacement of the bromine group. (**Figure 3.2**). The desired triazatruxene produced in this process can undergo further bromination to afford poly-brominated triazatruxenes, which are insoluble in most organic solvents. The crude product mixture was then used in the subsequent reductive de-bromination step.
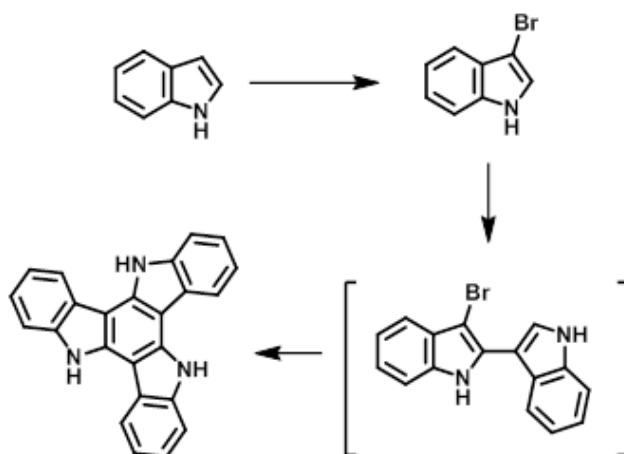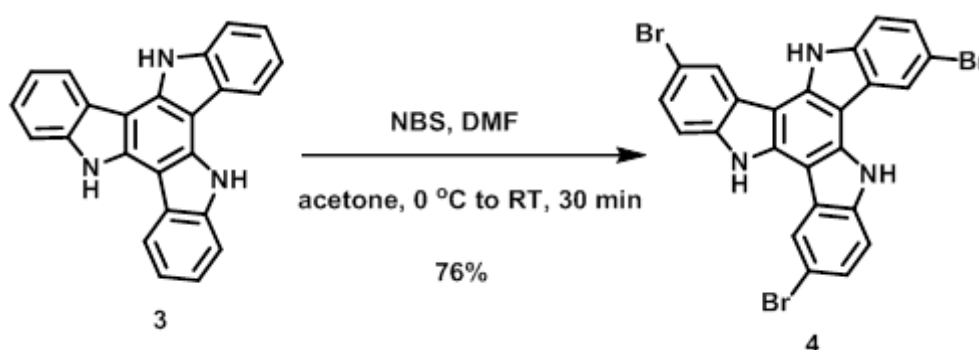

Figure 3.2 Br$_2$-catalyzed cyclotrimerisation of indole

The regioselective tribromination by using NBS in DMF at 0 °C provided tribromotriazatruxene in good yield of 76% (**Scheme 3.2**). The structure of **4** was confirmed by ¹H-NMR (**Figure 3.3**).

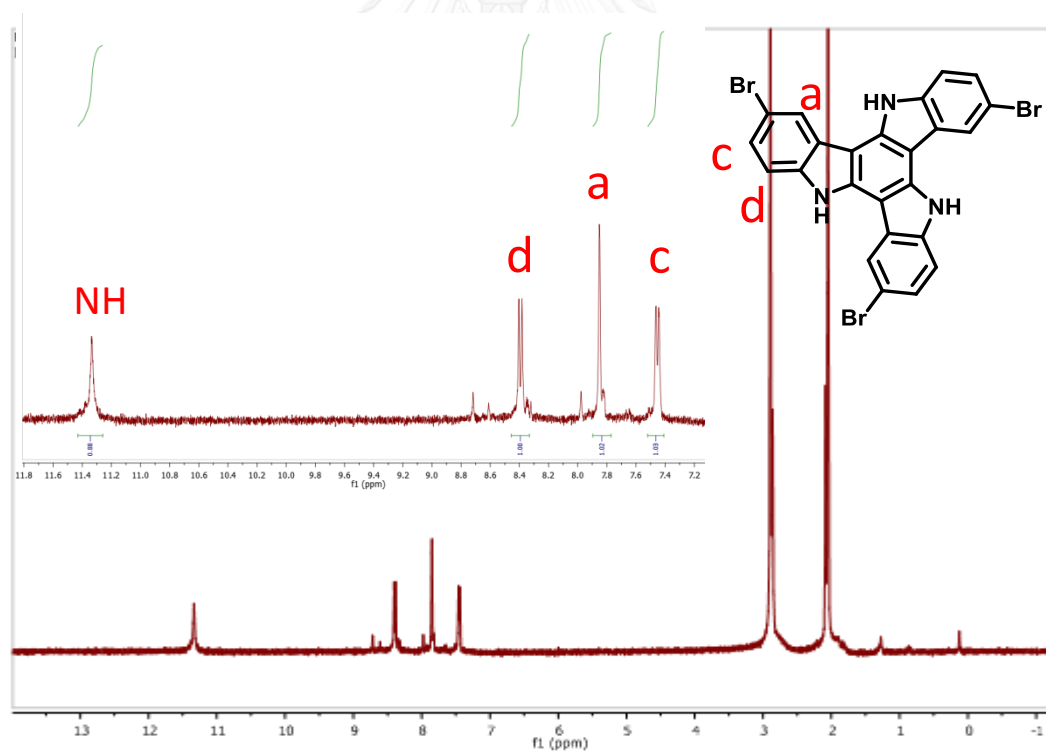**Scheme 3.2** The synthesis of tribromotriazatruxene (**4**)


Figure 3.3 ¹H-NMR of tribromotriazatruxene core (**4**) in acetone-d6

In the third step, the –NH group of triazatruxene was protected using different alkyl groups. Treatment of tribromo triazatruxene (**4**) with ethylhexylbromide and KOH in DMSO produced **5** in excellent yield of 95%, while the reaction with benzyl bromide under the phase-transfer catalysis gave rise to **6** in nearly quantitative yield (**Scheme 3.3**). Two desired intermediates were characterized by ^{1}H-NMR (**Figure 3.4a and Figure 3.4b**).
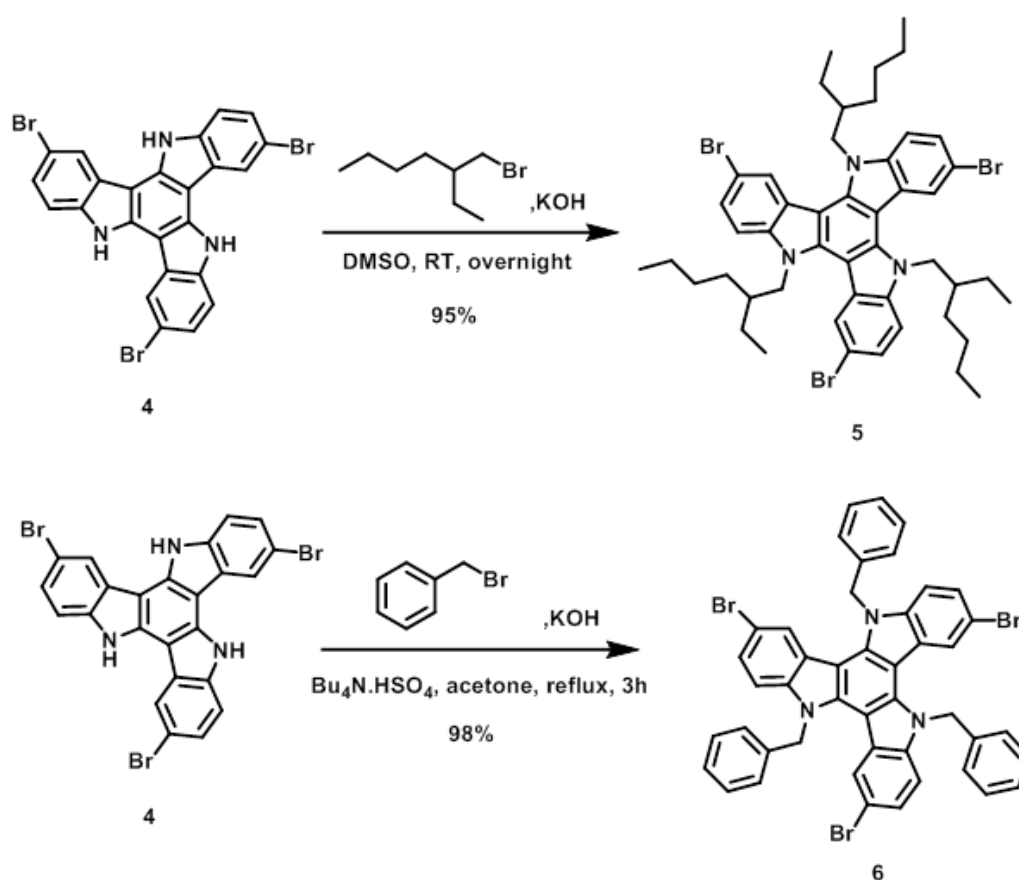
Scheme 3.3 The synthesis of **5** and **6**

According to the ^{1}H-NMR spectra (**Figure 3.4a** and **Figure 3.4b**), the signals of -CH_2N- protons in both compound **5** and **6** did not agree well with the theoretical prediction. These might result from the use of racemic ethylhexylbromide which resulted in a variety of diastereromers of **5**, or the restricted rotation of the benzyl group in **6**.
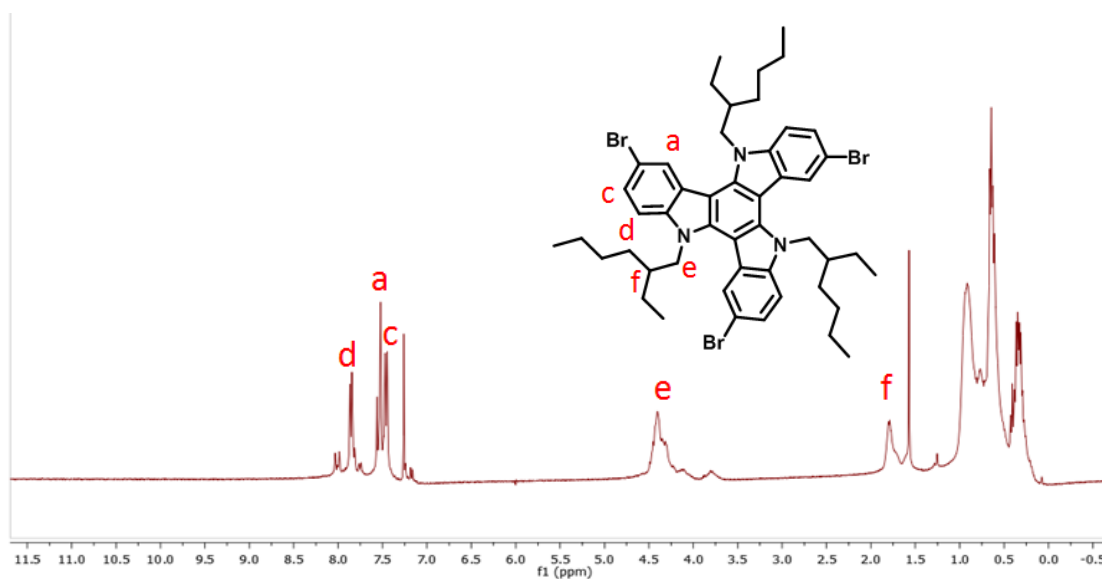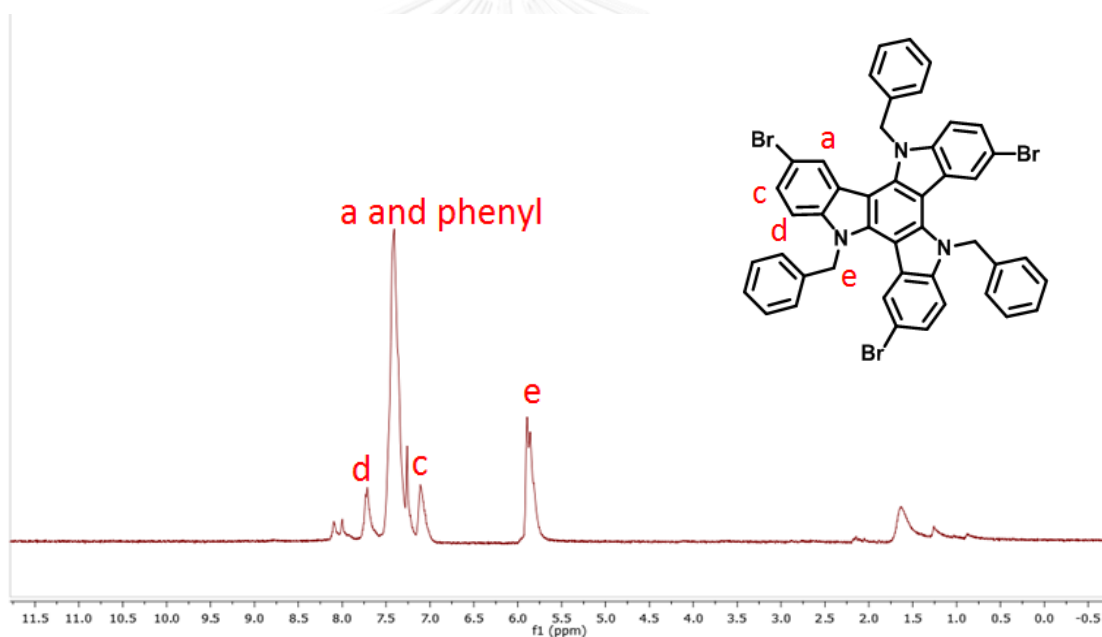
Figure 3.4a ^{1}H-NMR of **5** in CDCl$_3$

Figure 3.4b ^{1}H-NMR of **6** in CDCl$_3$

The last step of the synthesis of the target compounds (**TAT1**, **TAT2**) relied on Suzuki cross-coupling reactions. The mechanism of Suzuki-cross coupling reaction (**Figure 3.5**) involves three-step cycles: The first step is the oxidative addition of palladium to the halide to form the organopalladium species. Reaction with base gives intermediate *via* transmetalation with the boron-ate complex and generates

the organopalladium species. Reductive elimination of the desired products (**TAT1**, **TAT2**) restores the original palladium catalyst which completes the catalytic cycle.
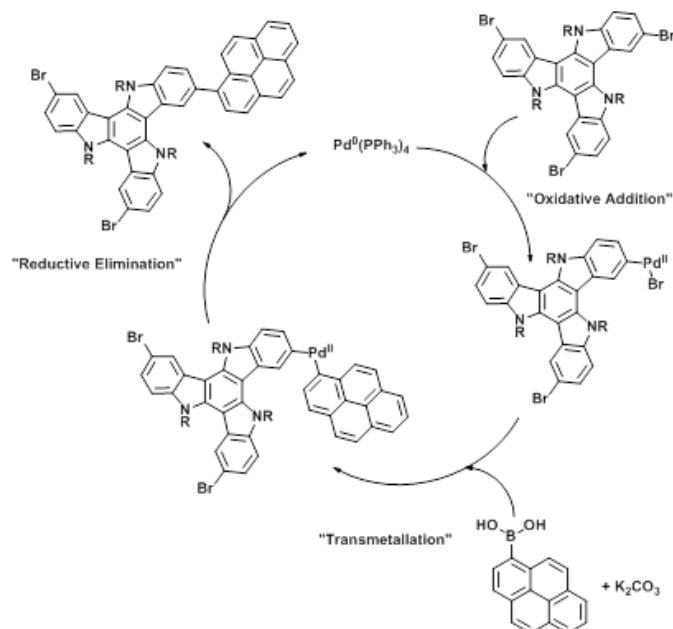

Figure 3.5 The mechanism of Suzuki cross-coupling

Three pyrene moieties were installed onto intermediate **5** and **6** using the Suzuki cross-coupling with pyrene-1-boronic acid in the present of Pd(PPh$_3$)$_4$ catalyst (**Scheme 3.4**) to produced **TAT1** and **TAT2**, respectively. These products were purified by silica chromatography and alumina chromatography to obtain desired products as yellow solids.
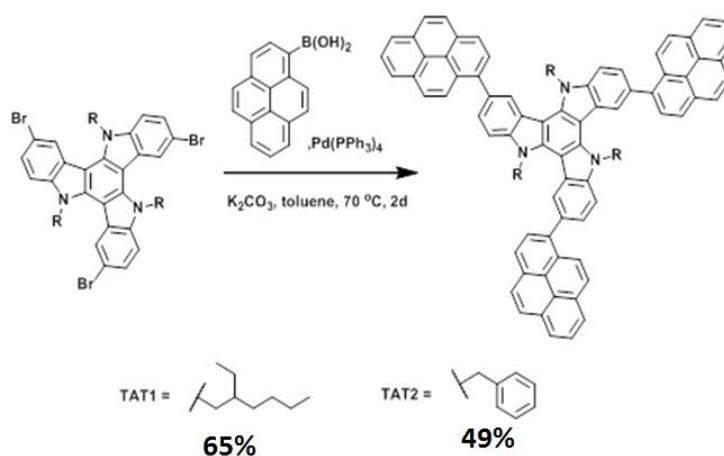
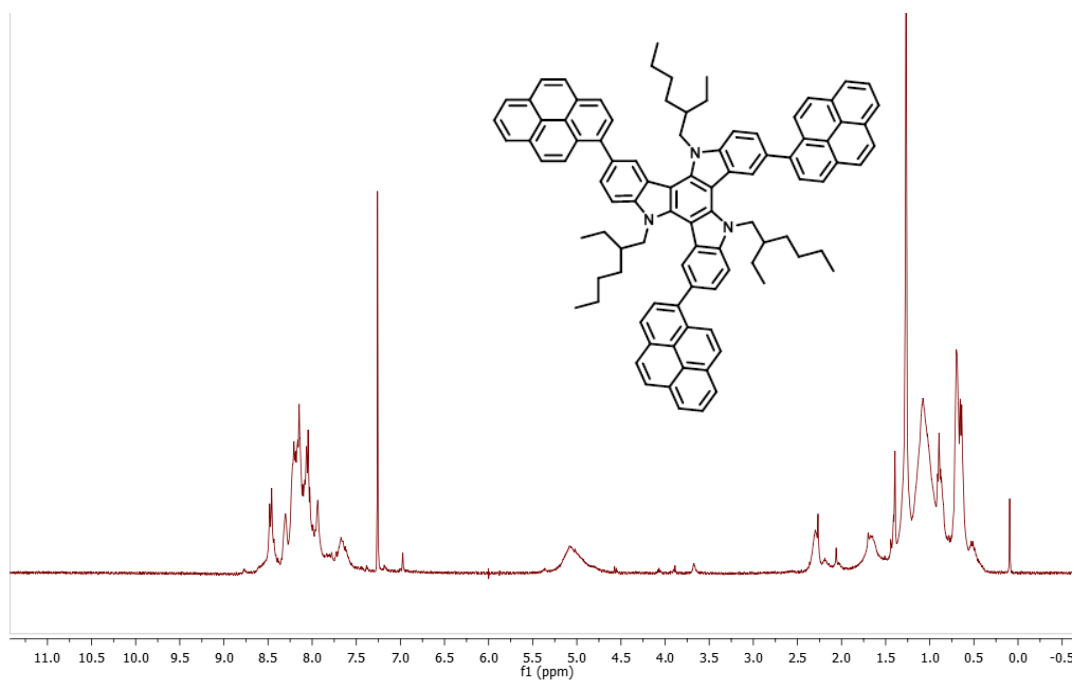**Scheme 3.4** The synthesis of **TAT1** and **TAT2**

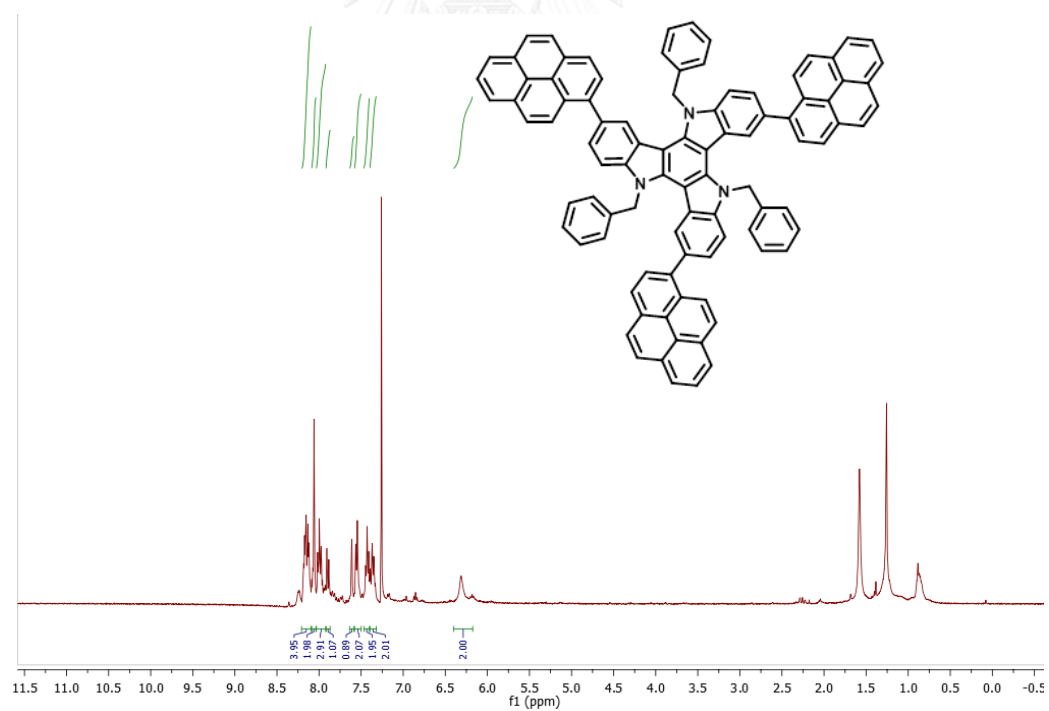**Figure 3.6a** ^{1}H-NMR of **TAT1** in CDCl$_3$

Figure 3.6b ^{1}H-NMR of **TAT2** in CDCl$_3$

3.2 Optical properties.

The investigation of absorption properties of **TAT1** and **TAT2** were performed in chloroform solution and solid state, respectively. The results are summarized in **Table 3.1**. In solution phase as shown in **Figure 3.7**, the absorption spectra of these triazatruxene derivatives exhibited the characteristic absorption peak of pyrene unit between 344-378 nm which corresponded to the π-π^* electron transition. Ethylhexyl substituted (**TAT1**) and benzyl substituted (**TAT2**) in solution phase had nearly identical absorption maxima (λ_{max}) at 344 and 351 nm, respectively. In solid state, the absorption maximum of **TAT2** showed a large red-shift compared with that of **TAT1** because of its aggregation effect by benzyl groups and planarity between the triazatruxene and pyrene units. Hence, the molar extinction coefficient of **TAT2** was higher than **TAT1** due to higher conjugation.
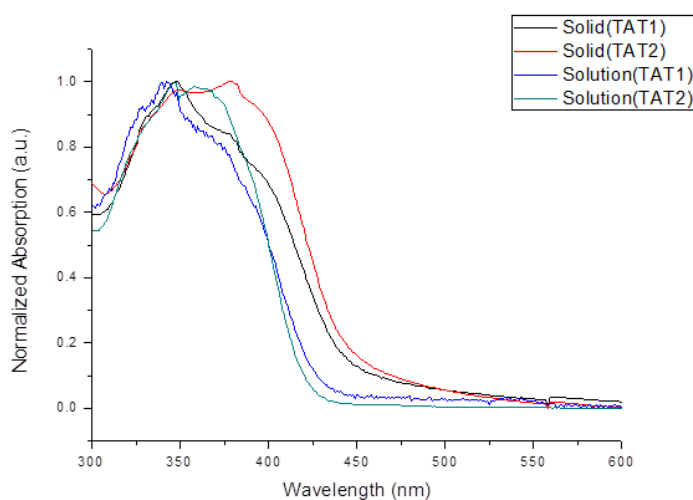

Figure 3.7 Normalized absorption spectra of **TAT1** and **TAT2** in CHCl$_3$ and thin film.

The normalized fluorescence spectra were shown in **Figure 3.8**, obtained from chloroform solution and solid state. In solution phase, **TAT1** and **TAT2** exhibited the maximum emission wavelength at 483 and 472 nm, respectively. The emission spectra of compound **TAT1** appeared at a slightly longer wavelength with higher quantum efficiency than **TAT2**. This might attribute to the steric hindrance of the three 2-ethylhexyl groups that enhanced the solubility in organic solvents and

prevented aggregation-caused fluorescent quenching. In solid state, emission spectra of desired compounds (**TAT1** and **TAT2**) exhibited a hypsochromic shift compared to the solution phase spectra. These results may also be attributed to the aforementioned solid-state packing force and the restricted structural relaxation. The quantum yields were measured in $CHCl_3$ solution at room temperature using quinine sulfate solution in 0.01 M H_2SO_4 ($\Phi_F = 0.54$) as a standard.
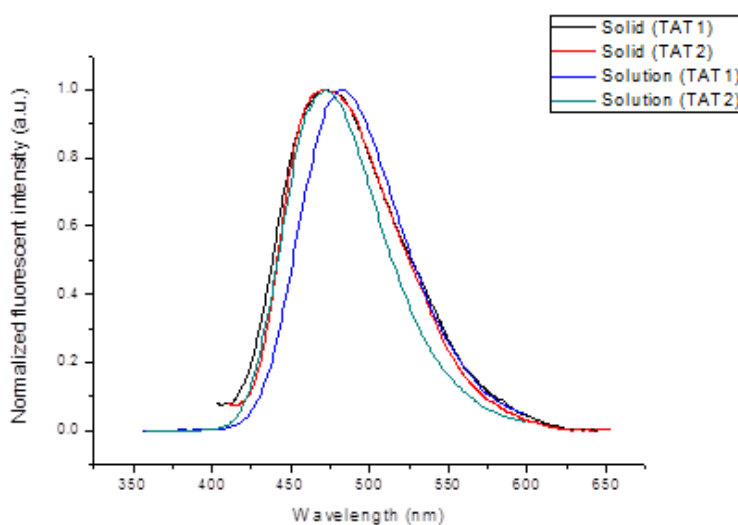

Figure 3.8 Normalized emission spectra of **TAT1** and **TAT2** in $CHCl_3$ and thin film.

Table 3.1 Photophysical properties of **TAT1** and **TAT2**.

Cpds.	Absorption			Emission		
	Solution[a]	Thin film[b]	log ε (M^{-1}cm^{-1})	Solution[c]	Thin film[d]	Φ_F[e]
TAT1	344	348	4.52	483	472	0.52
TAT2	351	378	4.88	472	471	0.61

[a] The absorption spectra from the UV-Vis spectra was measured in $CHCl_3$. [b] The absorption spectra from the UV-Vis spectra measured in thin film. [c] The PL emission excited at the absorption maxima in dilute $CHCl_3$ solution. [d] The PL emission excited at the absorption maxima in thin film. [e] PL quantum yield determined in $CHCl_3$ solution (A<0.1) at room temperature using quinine sulfate solution in 0.1 M H_2SO_4 ($\Phi_F = 0.54$) as a standard.

3.3 Electrochemical properties

      The electrochemical properties of **TAT1** and **TAT2** were also studied and their energy gaps between the highest occupied molecular orbital (HOMO) and the lowest unoccupied molecular orbital (LUMO) were obtained from cyclic voltammograms and UV-Vis absorption spectra. The data was shown in **Table 3.2**.

      From the UV-vis experiments, the optical band gap energy could be determined from the onset of absorption wavelength (the lowest energy that molecules absorb to excite the electron to the excited state) which was estimated by $E_g= 1240/\lambda_{onset}$. The onset absorption of **TAT1** and **TAT2** are 427 and 421 nm, respectively corresponding to band gap energy of 2.90 and 2.95 eV.

      In this CV experiments, platinum wire was used as a counter electrode, $Ag/AgNO_3$ as a reference electrode and glassy carbon as a working electrode, tetra-n-butylammonium hexafluorophosphate ($TBAPF_6$) as a electrolyte which solute in organic solvents. The concentrations of electrolyte and desired products (**TAT1** and **TAT2**) were 0.1 M, and 1.0 mM, respectively. (**Figure 3.9a** and **Figure3.9b**).
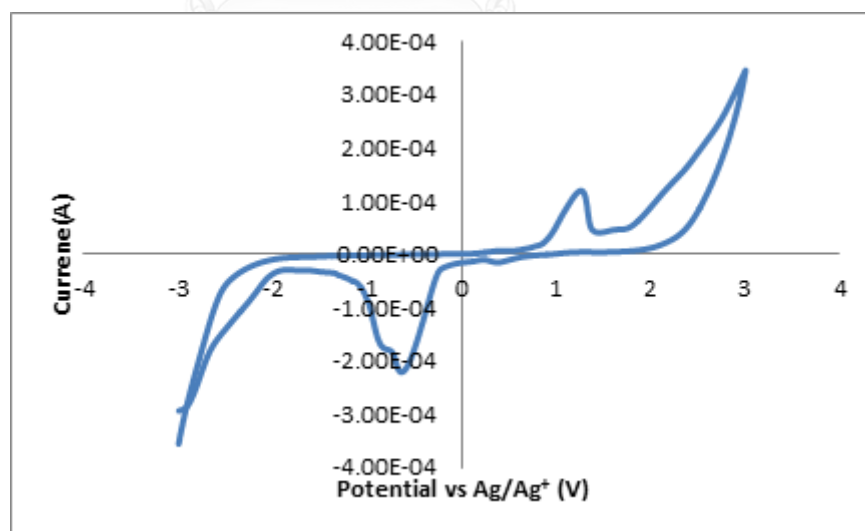

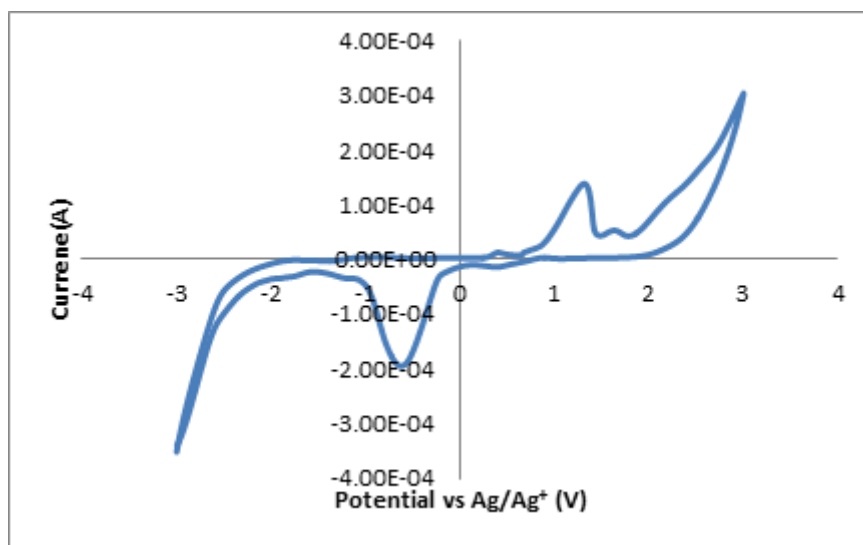**Figure 3.9a** Cyclic voltammograms of **TAT1** in CH_2Cl_2.

Figure 3.9b Cyclic voltammograms of **TAT2** in CH_2Cl_2.

The HOMO energy levels were calculated from the onset of oxidation potential (E_{onset}) according to a formula, HOMO = -(4.44+E_{onset}) [42, 43]. The LUMO energy levels were calculated by subtracting the HOMO energy levels with the band gaps energy estimated from the onset of UV−Vis absorption. The onsets of oxidation potential of **TAT1** and **TAT2** were at 0.87 and 0.90, respectively. These suggested that **TAT1** could be oxidized easier and have better hole-transporting than **TAT2**. The HOMO energy levels of all compounds were in the range of 5.31-5.34 eV, which were lower than ITO (4.80 eV) as shown in band diagram (**Figure 3.10**).
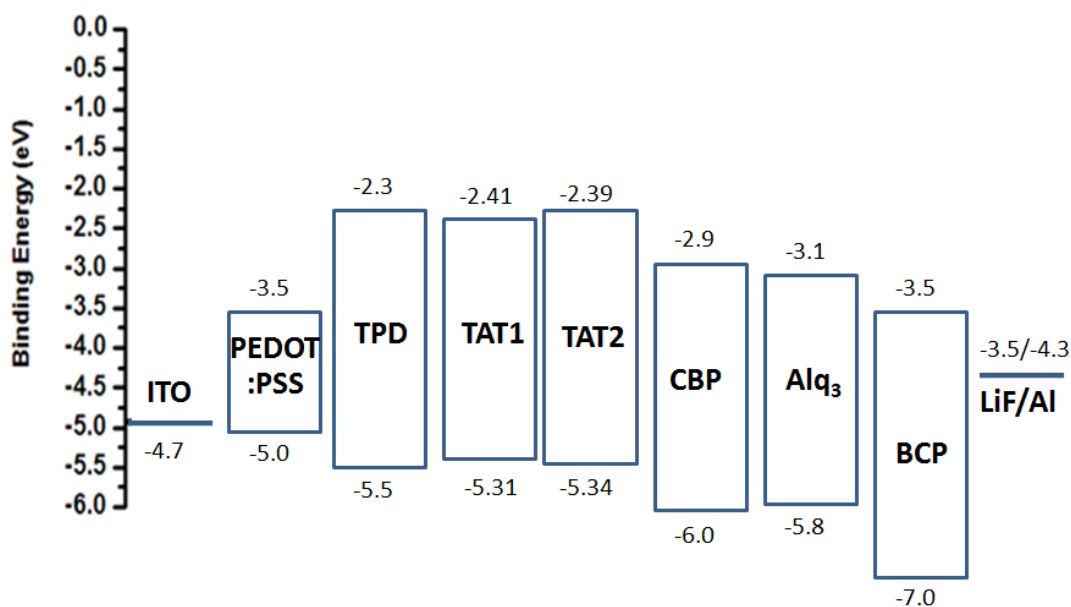
Figure 3.10 Band diagram of ITO, PEDOT:PSS, TPD, **TAT1**, **TAT2**, CBP, Alq₃, BCP and LiF:Al

The experimental and computationally calculated electrochemical properties are summarized in **Table 3.2**. The experimental HOMO and LUMO levels of two compounds were in the range of -5.15 to -5.16 eV and -1.68 to -1.74 eV, respectively. These energy levels obtained from the calculations using Gaussian 09 code with geometry optimizations using B3LYP/6-31G(d,p) method also agree with the experimental values. The orbital plots show exclusive electron localizations at the triazatruxene core for the HOMOs, and at the pyrene groups for the LUMOs (**Figure 3.11**).
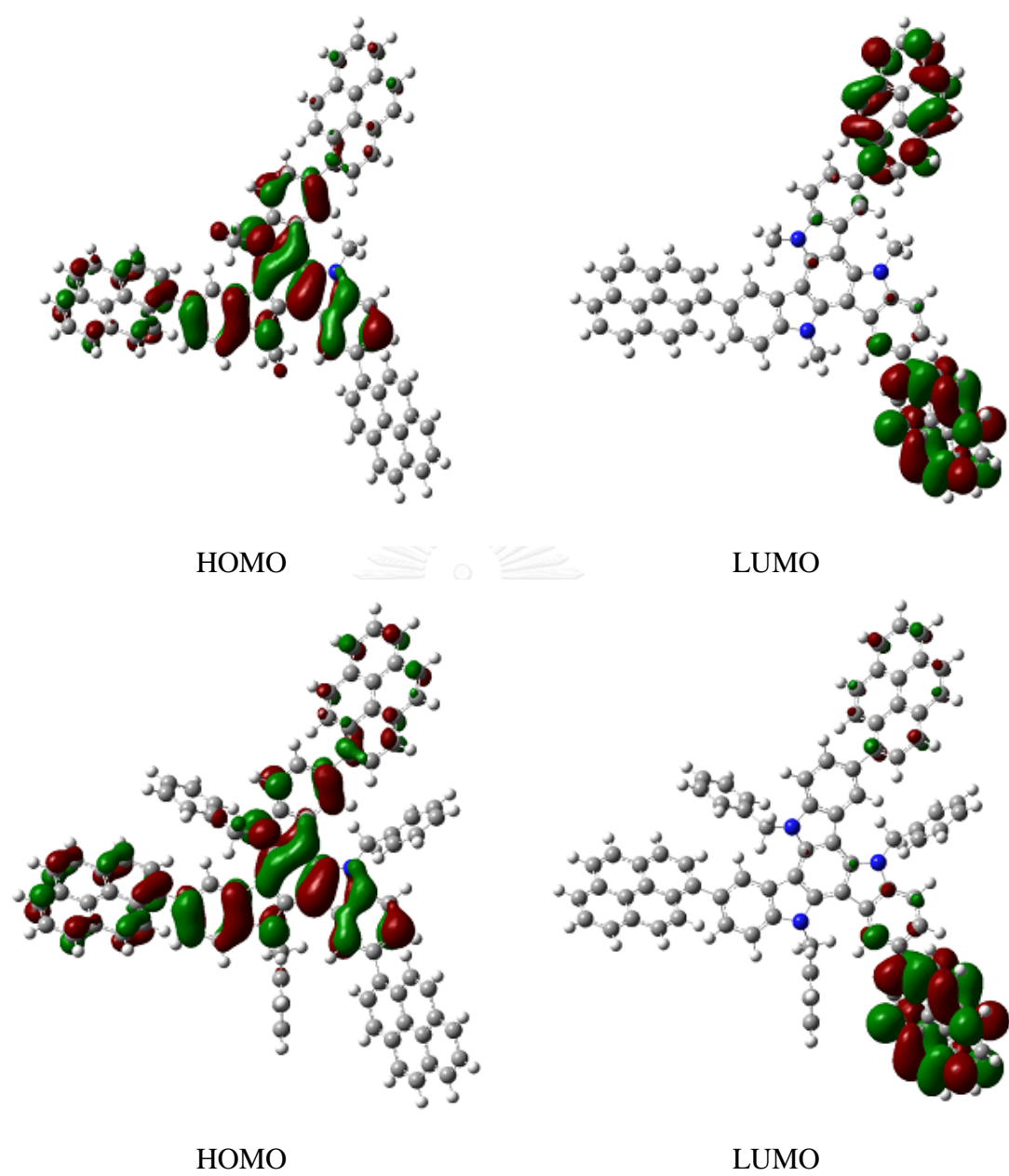
HOMO   LUMO

HOMO   LUMO

Figure 3.11 Frontier orbital plots for **TAT1**(top) and **TAT2**(bottom).

Table 3.2 The experimental and calculated electrochemical properties of **TAT1**, **TAT2**.

Cpds.	Experimental data			Calculated data[d]		
	HOMO (eV)[a]	LUMO (eV)[b]	E_g (eV)[c]	HOMO (eV)	LUMO (eV)	E_g (eV)
TAT1	-5.31	-2.41	2.90	-5.15	-1.74	3.41
TAT2	-5.34	-2.39	2.95	-5.16	-1.68	3.48

[a] Estimated by the empirical equation: HOMO = $-(4.44+E_{onset})$. [b] Estimated from LUMO = HOMO + E_g.[c] The optical energy gap estimated from the onset of the absorption spectra ($E_g = 1240/\lambda_{onset}$). [d] All calculations were performed by Gaussian 09 code and geometry optimizations were done by B3LYP/6-31G(d,p) method.

3.4 Thermal properties

For optoelectronic applications, the thermal stability of organic materials is crucial for device stability and lifetime. The degradation of organic optoelectronic devices depends on morphological changes resulting from the thermal stability of the amorphous organic layer. Morphological change might be promoted by rapid molecular motion near the glass transition temperature (T_g). The thermal properties of all compounds were determined by differential scanning calorimetry (DSC) and thermogravimetric analysis (TGA) under nitrogen atmosphere.

The thermal properties of **TAT1** and **TAT2** are shown in **Figure 3.12** and summarized in **Table 3.3**. The TGA curves revealed that two compounds were thermally stable with high 10% weight loss temperatures ($T_d{}^{10\%}$) at 310.7 and 262.7 ^{o}C, respectively. The excellent thermal stability with high T_d readily leads to high stability OLEDs, which is favorable to improve the performance and lifetime of OLEDs during operation. From DSC on second heating cycle, **TAT1** showed only an endothermic peak at 305.1 ^{o}C due to glass transition temperature (T_g) and no signal for melting (T_m) and crystallization temperature (T_c) was observed. For **TAT2** showed endothermic baseline shift at due to glass transition temperature (T_g) at

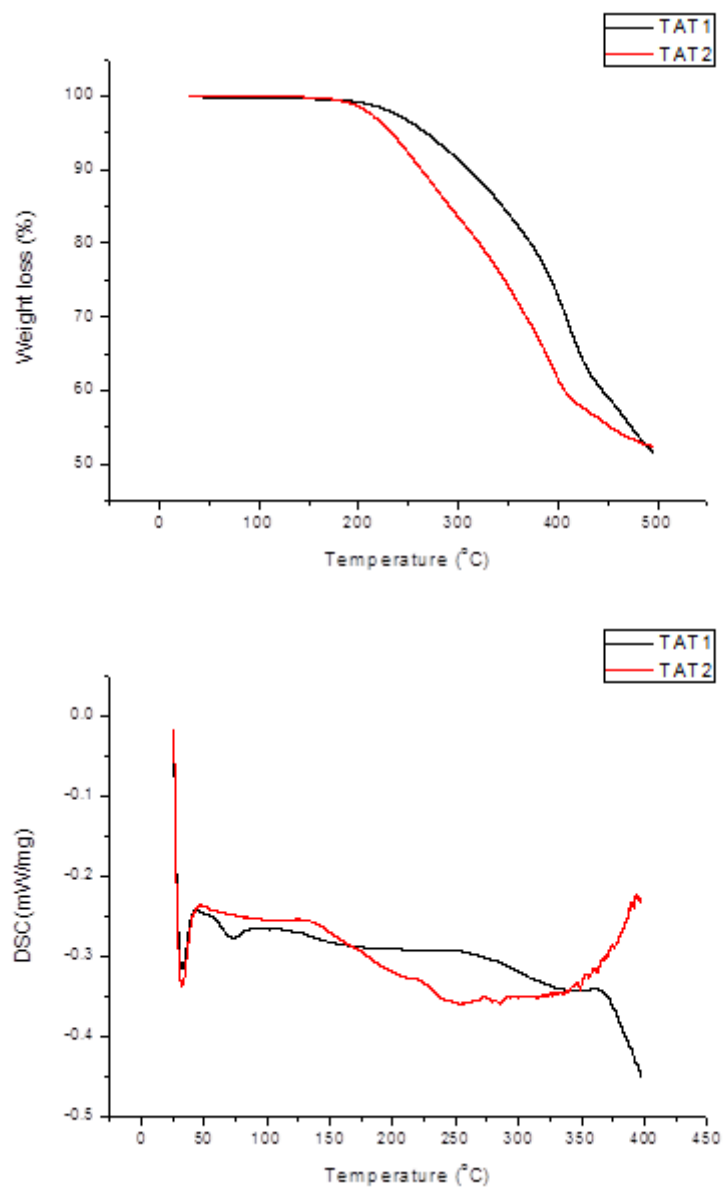231.7 ^{o}C. These results suggested that all compounds could form molecular glass with high T_g.

Figure 3.12 TGA (top) and DSC (bottom) traces of **TAT1** and **TAT2** measured under N$_2$ atmosphere at heating rate of 10°C/min.

Table 3.3 Thermal properties of **TAT1** and **TAT2**.

Compounds	T_g (^{o}C)[a]	T_d (^{o}C)[b]
TAT1	305.1	310.7
TAT2	231.7	262.7

[a] Obtained from DSC measurements on the second heating cycle with a heating rate of 10^oC/min under N_2. [b] 10% decomposition temperature obtained from TGA measurement with a heat rate of 10^oC/min under N_2.

3.5 Electroluminescent properties

3.5.1 Investigation of the hole-transporting property

The HOMO energies of **TAT1** and **TAT2** were at -5.31 and -5.34 eV, respectively. These energy levels lied between the work function of ITO (-4.80 eV) and HOMO energy of Alq_3 (-5.70 eV) which indicated that all compounds could potentially be used as a hole transporting layer (HTL) in OLED. For good performance, PEDOT:PSS (-5.00 eV) were used as hole injection layer (HIL) between anode and HTL. To investigate their hole-transporting properties, multi-layer OLED devices with the structure of ITO / PEDOT:PSS / HTL / Alq_3 / LiF / Al were fabricated by **TAT1** (device 3), **TAT2** (device 4) as the HTL. For device 2, **TPD**, commercial hole transporting material, was used as HTL to compare with our compounds and without HTL for device 1, ITO as the anode, LiF / Al as the cathode and Alq_3 as the light-emitting and electron-transporting layers. From the results, all devices emitted the green color of Alq_3 (518 nm) except device 3 because of its short circuit.
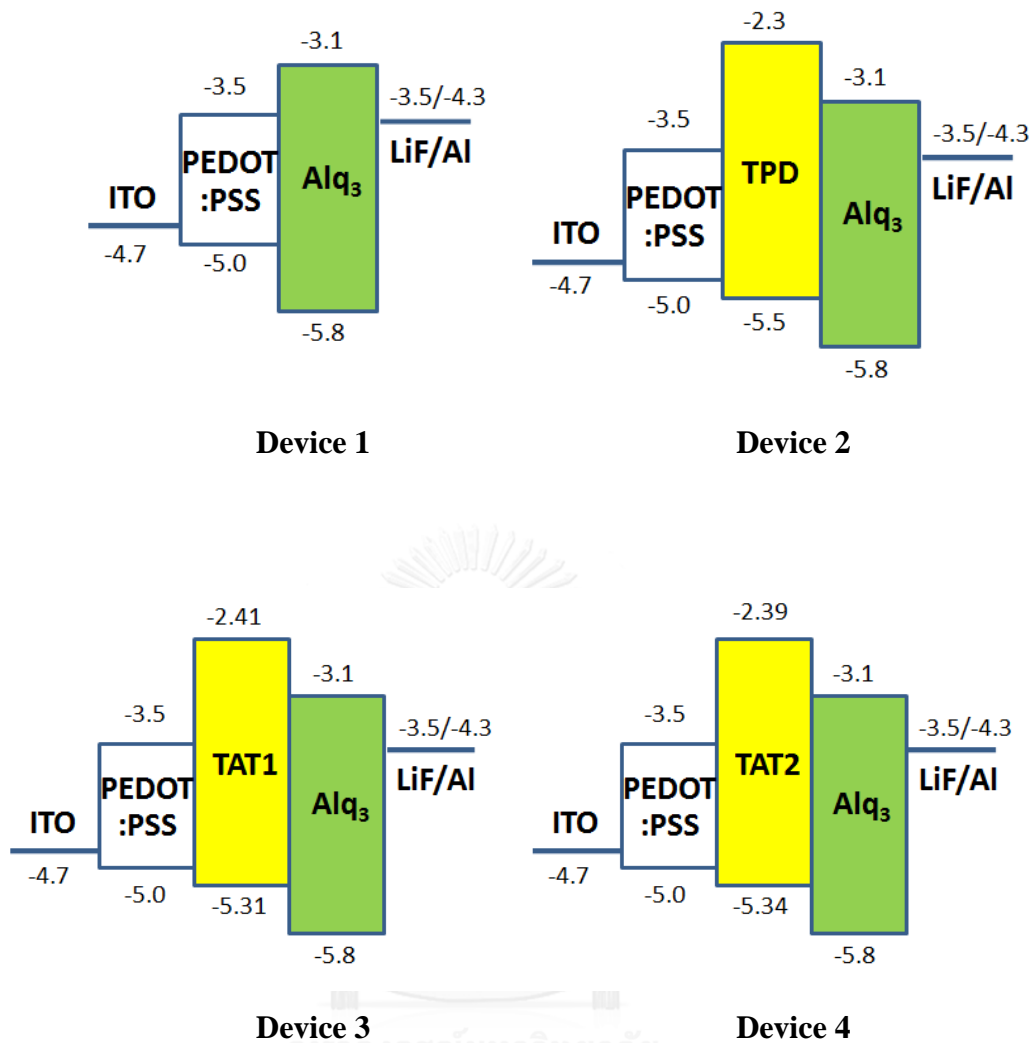
Figure 3.13 Energy level diagrams of device 1-4.

The voltage-luminance and voltage-current density characteristics of the devices are shown in **Figure 3.14** and summarized in **Table 3.4**. Device 4 exhibited the best performance with a maximum luminance of 31,971 cd/m^2 at 10.8 V, a turn-on voltage of 2.6 V and an external efficiency of 1.17%. This is possibly attributed to the fact that device 4 has charge balance better than the other two devices due to a small energy barrier between **TAT2** and ITO (**Figure 3.13**).
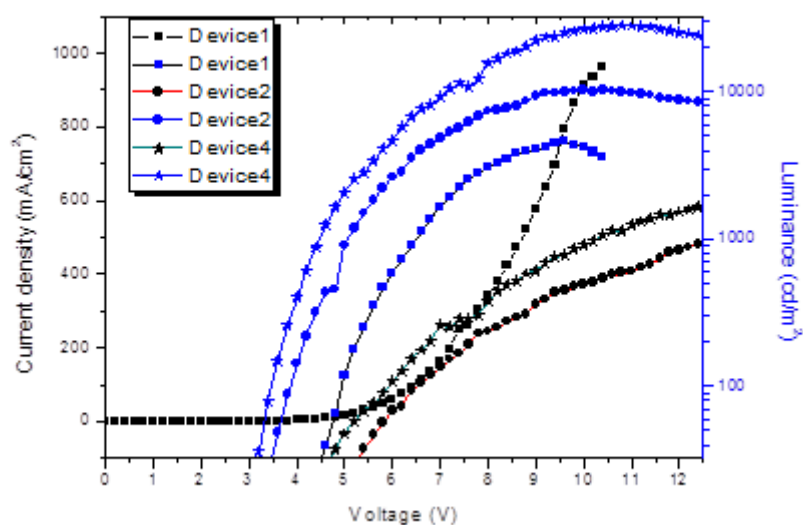
Figure 3.14 Current density and luminance VS voltage (*J-V-L*) characteristics of device 1, 2 and 4.

Table 3.4 Electroluminescent properties of device 1,2 and 4.

Device	V_{on}[a]	V_{max}	L_{max}[b]	J_{max}[c]	LE_{max}[d]	PE (lm/W)	%EQE[e]	CIE[f]
Device 1	4.0	9.6	4633	795	1.01/ 7.0V	0.52/ 5.6V	0.25/ 7.0V	0.297, 0.532
Device 2	2.6	10.8	11446	684	4.15/ 4.6V	3.55/ 3.0V	1.02/ 4.6V	0.276, 0.515
Device 4	2.6	10.8	31971	1297	4.76/ 5.2V	3.64/ 3.6V	1.17/ 5.2V	0.275, 0.515

[a] Turn-on voltage (V). [b] Maximum luminance (cd/m^2). [c] Current density (mA/m^2). [d] Luminance efficiency (cd/A) (at applied potential V). [e] External efficiency (%). [f] Commission International d'Eclairage coordinates (*x*, *y*).

3.5.2 Investigation of the electroluminescent property

The high photoluminescence (PL) quantum yields of **TAT1** and **TAT2** motivated us to use these compounds as light-emitting layers for OLED. The exploration of light-emitting properties was divided into three parts. The concentration of **TAT2** was the first priority to study. Their functions were emissive material layer (EML) in devices of structure ITO / PEDOT:PSS / EML / BCP / LiF / Al which the appropriate concentrations were investigated to fabricate multi-layer OLED device. Weight per volume of 1.5, 3.0 and 4.5 were chosen to study. Unfortunately, those concentrations were abuse because they caused the short circuit under the applied voltage. Further study, the type of solvents was concerned as a great point in evaporation property. The slow rate of evaporation could decrease the crystallization. The more crystallization rose up, the easier short circuit occurred. Therefore, the ratio of chloroform and toluene were varied. The variety of ratios chloroform to toluene were 2:1 and 1:2, respectively. Regrettably, the trials were failed which resulted in short circuit. From which the above problems, the alternative solution was considered as doped EML with CBP. Based on hypothesis, doped EML with CBP could decrease the concentration of substrate and crystallinity. On the contrary, doped EML with CBP could increase amorphous. The 5 and 10% w/w of doped EML with CBP were examined for the optimum. Device 5 and 6 were recognized as 5 and 10% w/w of doped **TAT1** with CBP, respectively whereas device 7 and 8 were designed for 5 and 10% w/w of doped **TAT2** with CBP, respectively (**Figure 3.15**). The voltage-luminance and voltage-current density characteristics of the devices are shown in **Figure 3.16** and summarized in **Table 3.5**. From the results, device 7 exhibited the highest performance with a maximum luminance of 5,666 cd/m^2 at 19.8 V, a turn-on voltage at 8.1 V and an external efficiency 2.01%. The results showed that **TAT2** can be used in EML better than **TAT1**.
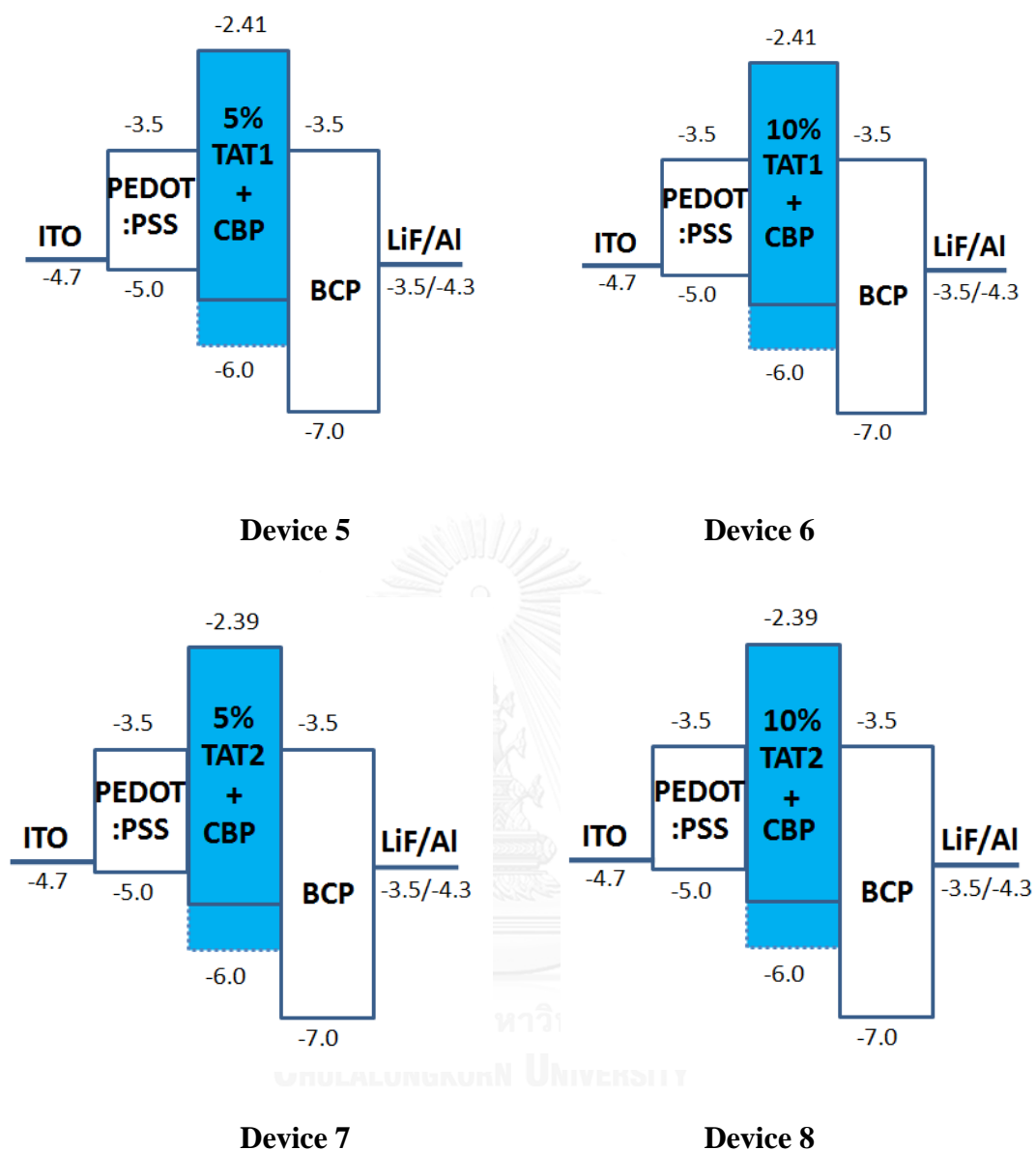
Device 5

Device 6

Device 7

Device 8

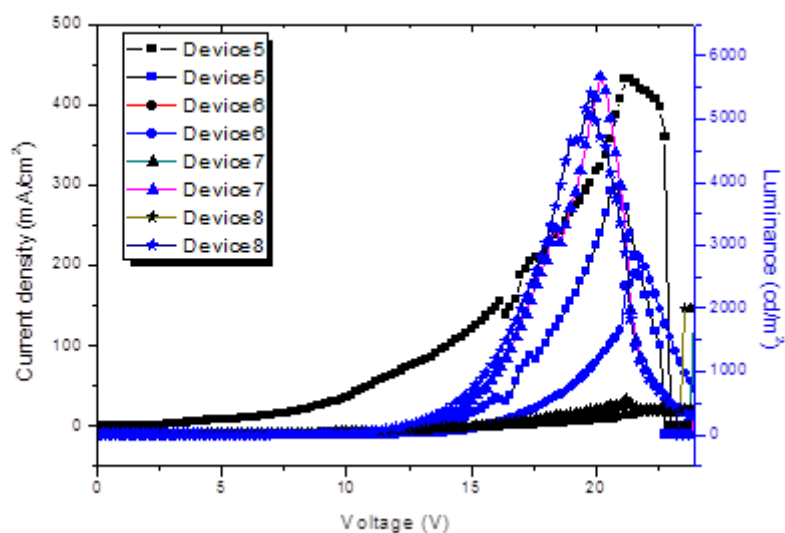**Figure 3.15** Energy level diagrams of device 5-8.

Figure 3.16 Current density and luminance VS voltage (*J-V-L*) characteristics of device 5-8.

Table 3.5 Electroluminescent properties of device 5-8.

Device	V_{on}[a]	V_{max}	L_{max}[b]	J_{max}[c]	LE_{max}[d]	PE (lm/W)	%EQE[e]	CIE[f]
Device 5	8.6	20.8	3910	388	1.08/ 20.6V	0.16/ 20.6V	1.49/ 20.6V	0.197, 0.300
Device 6	10.0	21.8	2789	335	0.83/ 21.8V	0.12/ 21.8V	1.15/ 21.8V	0.197, 0.283
Device 7	8.1	20.2	5666	393	1.46/ 19.8V	0.23/ 19.8V	2.01/ 19.8V	0.172, 0.252
Device 8	6.8	19.8	5410	392	1.42/ 19.6V	0.23/ 19.0V	1.97/ 19.6V	0.172, 0.253

[a] Turn-on voltage (V). [b] Maximum luminance (cd/m^2). [c] Current density (mA/m^2). [d] Luminance efficiency (cd/A) (at applied potential V). [e] External efficiency (%). [f] Commission International d'Eclairage coordinates (*x*, *y*).

The electroluminescent (EL) spectra of the devices are shown in **Figure 3.17**. The EL peaks of devices 5-8 were at 478, 478, 473 and 473 nm, respectively. For PL spectra (**Figure 3.18**), the emissions of **TAT1** and **TAT2** were at

472 and 471, respectively. However, for **TAT1** and **TAT2** doped with CBP, the PL spectra showed hypsochromic shift in comparison to **TAT1** and **TAT2** with non-doped. Since CBP was intercalated between **TAT1** or **TAT2** which could decrease conjugation.
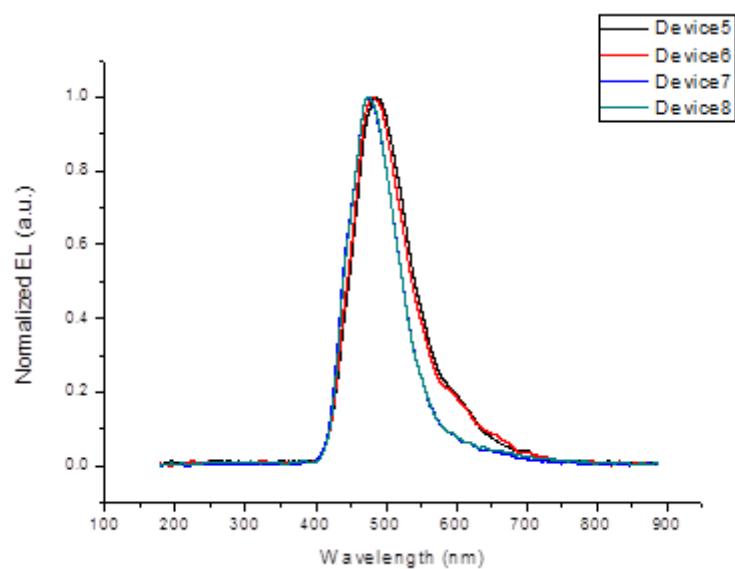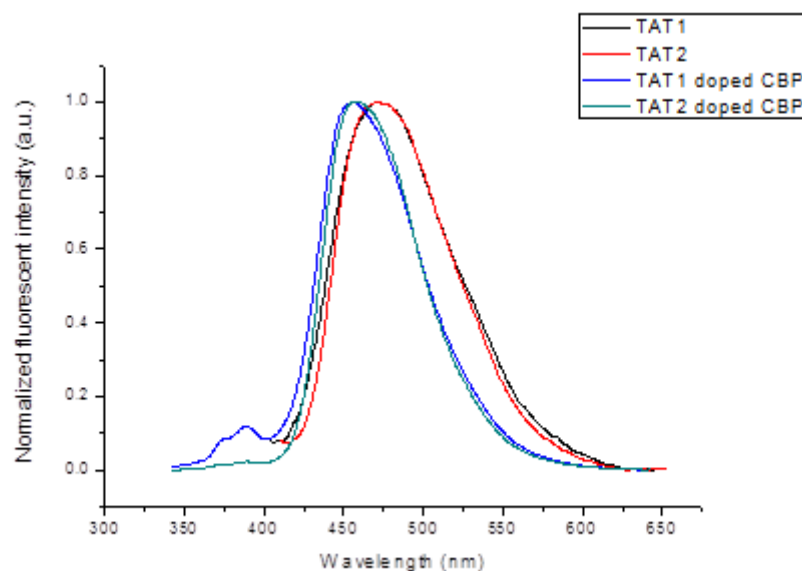

Figure 3.17 EL spectra of device 5-8.

Figure 3.18 PL spectra of **TAT**1 and **TAT2** with doped and non-doped in thin film.

The Commission International d'Eclairage (CIE) coordinates for device 5-8 were in the pure blue region as shown in **Figure 3.19** and summarized in **Table 3.5**.
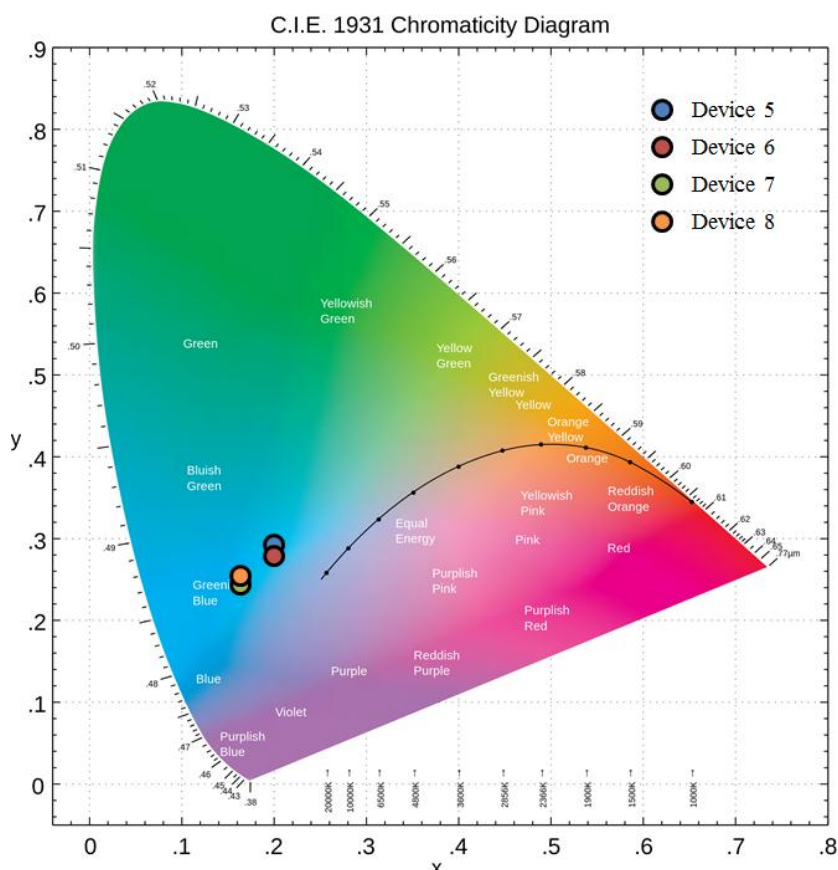
Figure 3.19 CIE coordination (x,y) of device 5-8.

AFM was used to measure the roughness of sample surfaces at high resolution which are shown in **Figure 3.20**. All four spin coating categories, TAT1, TAT1 doped with CBP, **TAT2** and **TAT2** doped with CBP at concentration of 0.3 %w/v were studied by using mixed solvent $CHCl_3$ and toluene at ratio 2:1. From the results, the rough surfaces of **TAT1** (a) and **TAT2** (c) are shown because the crystallinity property. On the other hand, the amorphous caused **TAT1** doped with CBP (b) and **TAT2** doped with CBP (d) were smoother than **TAT1** (a) and **TAT2** (b). The appearance of crystallinity could cause the short curcuit. Therefore, the amorphous was required for HTL and EML fabrication as an alternative solution to solve the short circuit problem.
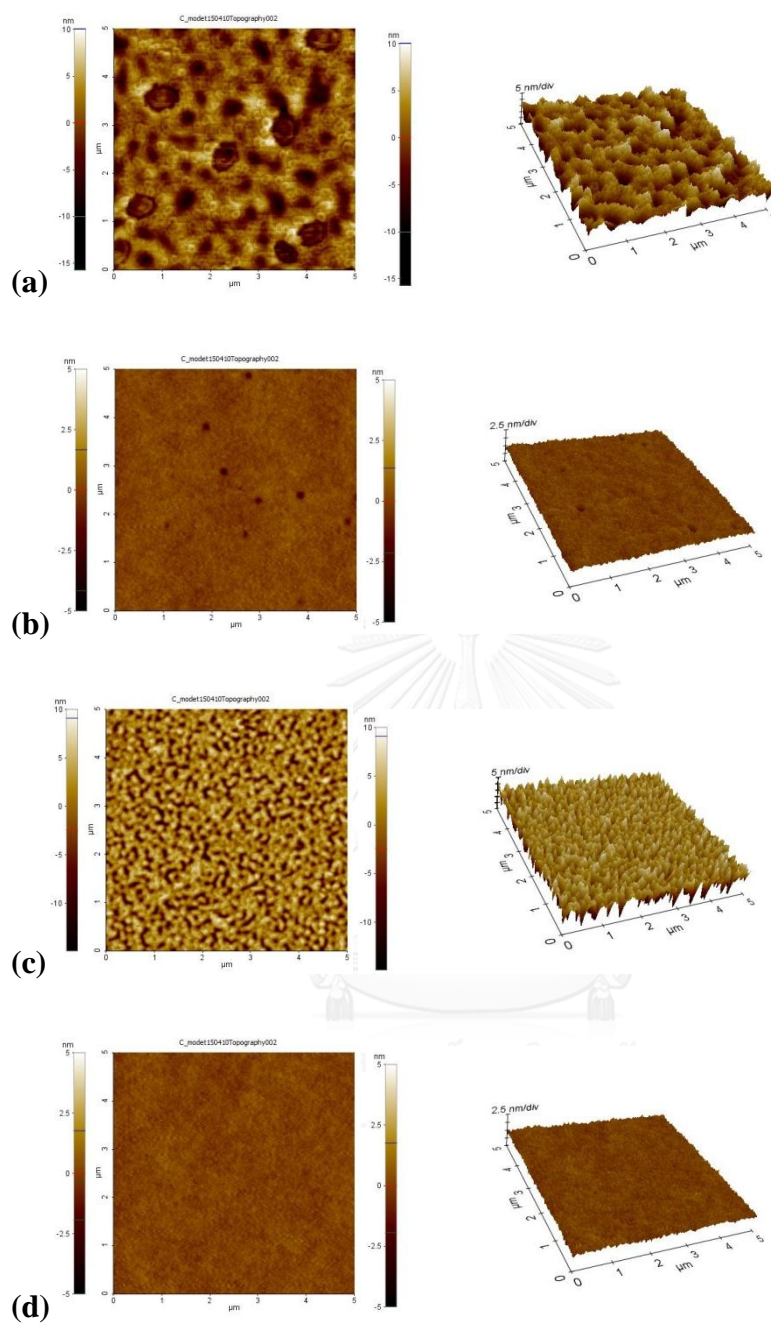
Figure 3.20 AFM images of (a) **TAT1**, (b) **TAT1** doped with CBP, (c) **TAT2** and (d) **TAT2** doped with CBP by spin coating.

CHAPTER IV
CONCLUSION

Two new symmetrical pyrenyl triazatruxene derivatives were successfully synthesized *via* Br_2-catalyzed cyclotrimerization of indole and Suzuki cross-coupling with pyrene-1-boronic acid. The substitution of the -NH position by 2-ethylhexyl and benzyl groups could prevent the aggregation by pi-stacking. All compounds were characterized by NMR spectroscopy, UV-Vis and fluorescence spectrophotometry and MALDI-TOF spectrometry. In $CHCl_3$ solutions, these compounds exhibited maximum absorption and emission around 344-351 nm and 472-483 nm, respectively. The hypsochromic shifts of both absorption and emission bands, along with narrower Stoke shifts in solid state spectra, may result from the solid-state packing and more restricted structural relaxation. The electrochemical investigation by cyclic voltammetry (CV) suggested that the HOMO energy level of **TAT1** and **TAT2** were at -5.15 and -5.16 eV, while the LUMO energy level were at -1.74 and -1.68 eV, respectively. Thermal properties were determined by differential scanning calorimetry (DSC) and thermogravimetric analysis (TGA) under nitrogen atmosphere. Both compounds exhibited excellent thermal stabilities with high glass transition temperatures (T_g) and decomposition temperature (T_d) above 230 ℃ and 305 ℃, respectively. OLED devices structures $ITO/PEDOT:PSS/TAT2/Alq_3/LiF:Al$ were fabricated to study their hole-transporting properties. The performance of **TAT2** was three-time better than that of TPD, which exhibited a bright green emission with a maximum luminescence of 31,971 cd/m^2 at 5.2 V and a turn-on voltage of 2.6 V. When CBP-doped **TAT2** was used as an emissive material in the OLED device of structure ITO/PEDOT:PSS/TAT2:CBP/BCP/LiF:Al, a blue light with a maximum brightness of 5,666 cd/m^2 were produced at the applied voltage of 19.8 V.

REFERENCES

[1]   Weiss, D.S. and Abkowitz, M. Advances in organic photoconductor technology. Chemical reviews 110(1) (2009): 479-526.

[2]   Geffroy, B., Le Roy, P., and Prat, C. Organic light-emitting diode (OLED) technology: materials, devices and display technologies. Polymer International 55(6) (2006): 572-582.

[3]   Zhu, F. OLED Activity and technology development. in Symposium on Sustainability Driven Innovative Technologies, 2009.

[4]   Chen, C.H., Tang, C.W., Shi, J., and Klubek, K.P. Green organic electroluminescent devices. 2000, Google Patents.

[5]   Tang, C.W. and VanSlyke, S.A. Organic electroluminescent diodes. Applied Physics Letters 51(12) (1987): 913-915.

[6]   Braun, D. and Heeger, A.J. Visible light emission from semiconducting polymer diodes. Applied Physics Letters 58(18) (1991): 1982-1984.

[7]   Braun, D. and Heeger, A. Electroluminescence from light-emitting diodes fabricated from conducting polymers. Thin Solid Films 216(1) (1992): 96-98.

[8]   Drury, C., Mutsaers, C., Hart, C., Matters, M., and De Leeuw, D. Low-cost all-polymer integrated circuits. Applied Physics Letters 73(1) (1998): 108-110.

[9]   Bao, Z., Lovinger, A.J., and Brown, J. New air-stable n-channel organic thin film transistors. Journal of the American Chemical Society 120(1) (1998): 207-208.

[10]   Zhao, T., Liu, Z., Song, Y., Xu, W., Zhang, D., and Zhu, D. Novel diethynylcarbazole macrocycles: synthesis and optoelectronic properties. The Journal of organic chemistry 71(19) (2006): 7422-7432.

[11]   Giro, G., et al. The role played by cell configuration and layer preparation in LEDs based on hydroxyquinoline metal complexes and a triphenyl-diamine derivative (TPD). Synthetic metals 102(1) (1999): 1018-1019.

[12]   Fang, Q., et al. A novel fluorene derivative containing four triphenylamine groups: Highly thermostable blue emitter with hole-transporting ability for organic light-emitting diode (OLED). Synthetic metals 155(1) (2005): 206-210.

[13] Sharma, A., Singh, D., Makrandi, J., Kamalasanan, M., Shrivastva, R., and Singh, I. Fabrication and characterization of OLED with Mg complex of 5-chloro-8-hydroxyquinoline as emission layer. Materials Chemistry and Physics 108(2) (2008): 179-183.

[14] Son, S.-H., et al. Electroluminescence characteristics of a novel biphenyl derivative with benzoxazole for organic light-emitting diodes. Current Applied Physics 5(1) (2005): 75-78.

[15] Ko, C.-W. and Tao, Y.-T. 9, 9-Bis {4-[di-(p-biphenyl) aminophenyl]} fluorene: a high T g and efficient hole-transporting material for electroluminescent devices. Synthetic metals 126(1) (2002): 37-41.

[16] Ren, X., et al. Organometallic complexes as hole-transporting materials in organic light-emitting diodes. Inorganic chemistry 43(5) (2004): 1697-1707.

[17] Chen, C.-H., Shen, W.-J., Jakka, K., and Shu, C.-F. Synthesis and characterization of spiro (adamantane-2, 9′-fluorene)-based triaryldiamines: thermally stable hole-transporting materials. Synthetic metals 143(2) (2004): 215-220.

[18] Zhi-feng, Z., Zhen-bo, D., Dong, G., Chun-jun, L., and Peng, L. Improved performance of organic light-emitting devices with 2-(4-biphenyl)-5-(4-butylphenyl)-1, 3, 4-oxadiazole. Displays 26(3) (2005): 133-136.

[19] Kao, P.-C., Chu, S.-Y., You, Z.-X., Liou, S., and Chuang, C.-A. Improved efficiency of organic light-emitting diodes using CoPc buffer layer. Thin Solid Films 498(1) (2006): 249-253.

[20] Lichtman, J.W. and Conchello, J.-A. Fluorescence microscopy. Nature methods 2(12) (2005): 910-919.

[21] Chen, C.-T. Evolution of red organic light-emitting diodes: materials and devices. Chemistry of Materials 16(23) (2004): 4389-4400.

[22] Mu, H., Li, W., Jones, R., Steckl, A., and Klotzkin, D. A comparative study of electrode effects on the electrical and luminescent characteristics of Alq 3/TPD OLED: Improvements due to conductive polymer (PEDOT) anode. Journal of Luminescence 126(1) (2007): 225-229.

[23] Pei, Q. and Yang, Y. Efficient photoluminescence and electroluminescence from a soluble polyfluorene. Journal of the American Chemical Society 118(31) (1996): 7416-7417.

[24] Grice, A., Bradley, D., Bernius, M., Inbasekaran, M., Wu, W., and Woo, E. High brightness and efficiency blue light-emitting polymer diodes. Applied Physics Letters 73(5) (1998): 629-631.

[25] Su, S.-J., Cai, C., Takamatsu, J., and Kido, J. A host material with a small singlet–triplet exchange energy for phosphorescent organic light-emitting diodes: Guest, host, and exciplex emission. Organic Electronics 13(10) (2012): 1937-1947.

[26] Fu, Q., Chen, J., Shi, C., and Ma, D. Solution-processed small molecules as mixed host for highly efficient blue and white phosphorescent organic light-emitting diodes. ACS applied materials & interfaces 4(12) (2012): 6579-6586.

[27] Song, M.-S., Nguyen, Q.P.B., Song, C.-H., Lee, D., and Chai, K.Y. Synthesis of Some Green Dopants for OLEDs Based on Arylamine 2, 3-disubstituted Bithiophene Derivatives. Molecules 18(11) (2013): 14033-14041.

[28] Burroughes, J., et al. Light-emitting diodes based on conjugated polymers. nature 347(6293) (1990): 539-541.

[29] Heeger, A.J. and Braun, D. Visible light emitting diodes fabricated from soluble semiconducting polymers. 1995, Google Patents.

[30] Huang, Q., Evmenenko, G.A., Dutta, P., Lee, P., Armstrong, N.R., and Marks, T.J. Covalently bound hole-injecting nanostructures. Systematics of molecular architecture, thickness, saturation, and electron-blocking characteristics on organic light-emitting diode luminance, turn-on voltage, and quantum efficiency. Journal of the American Chemical Society 127(29) (2005): 10227-10242.

[31] Lee, J.Y., Park, J.-Y., Min, S.-H., Lee, K.-W., and Baek, Y.G. A thermally stable hole injection material for use in organic light-emitting diodes. Thin Solid Films 515(20) (2007): 7726-7731.

[32] Promarak, V., Ichikawa, M., Sudyoadsuk, T., Saengsuwan, S., Jungsuttiwong, S., and Keawin, T. Synthesis of electrochemically and thermally stable

amorphous hole-transporting carbazole dendronized fluorene. <u>Synthetic metals</u> 157(1) (2007): 17-22.

[33] Raksasorn, D. <u>Derivatives of Carbazole and Truxene for Organic Light-Emitting Diodes</u>. M.Sc., Department of Chemistry Chulalongkorn University, 2012.

[34] Feng, G.-L., Lai, W.-Y., Ji, S.-J., and Huang, W. Synthesis of novel star-shaped carbazole-functionalized triazatruxenes. <u>Tetrahedron letters</u> 47(39) (2006): 7089-7092.

[35] Lai, W.-Y., Zhu, R., Fan, Q.-L., Hou, L.-T., Cao, Y., and Huang, W. Monodisperse six-armed triazatruxenes: Microwave-enhanced synthesis and highly efficient pure-deep-blue electroluminescence. <u>Macromolecules</u> 39(11) (2006): 3707-3709.

[36] Zhu, T., He, G., Chang, J., Zhao, D., Zhu, X., and Zhu, H. The synthesis, photophysical and electrochemical properties of a series of novel 3, 8, 13-substituted triindole derivatives. <u>Dyes and Pigments</u> 95(3) (2012): 679-688.

[37] Williams, A.T.R., Winfield, S.A., and Miller, J.N. Relative fluorescence quantum yields using a computer-controlled luminescence spectrometer. <u>Analyst</u> 108(1290) (1983): 1067-1071.

[38] Franceschin, M., Ginnari-Satriani, L., Alvino, A., Ortaggi, G., and Bianco, A. Study of a convenient method for the preparation of hydrosoluble fluorescent triazatruxene derivatives. <u>European Journal of Organic Chemistry</u> 2010(1) (2010): 134-141.

[39] Warf, A. <u>Negative Dryfilm Photo resist manual</u> Negative Dryfilm 2004. Available from: <u>http://www.warf.com.html</u>

[40] Wright, W.D. A re-determination of the trichromatic coefficients of the spectral colours. <u>Transactions of the Optical Society</u> 30(4) (1929): 141.

[41] Guild, J. The colorimetric properties of the spectrum. Philosophical Transactions of the Royal Society of London. Series A, Containing Papers of a Mathematical or Physical Character (1932): 149-187.

[42]   Yang, F., et al. Enhanced electroluminescent properties of triarylamine-endcapped X-branched oligofluorene. Synthetic metals 158(21) (2008): 988-992.

[43]   Zhu, W., Hu, M., Yao, R., and Tian, H. A novel family of twisted molecular luminescent materials containing carbazole unit for single-layer organic electroluminescent devices. Journal of Photochemistry and Photobiology A: Chemistry 154(2) (2003): 169-177.

APPENDIX
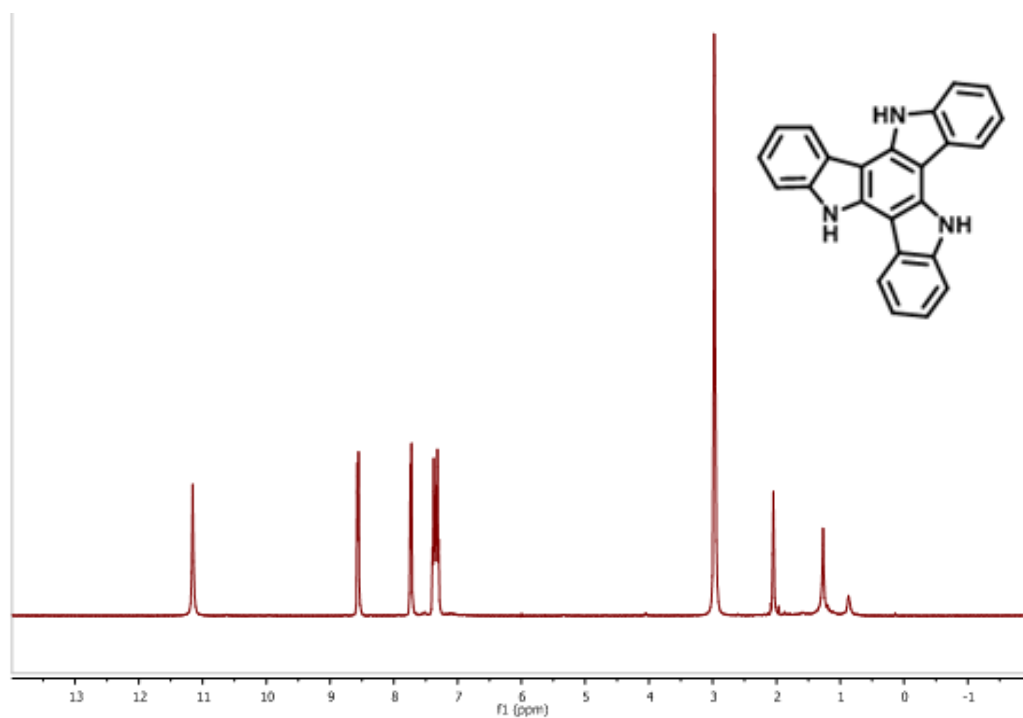
Figure A1. ¹H-NMR of 10,15-dihydro-5H-diindolo[3,2-a:3',2'-c]carbazole in acetone-d6.
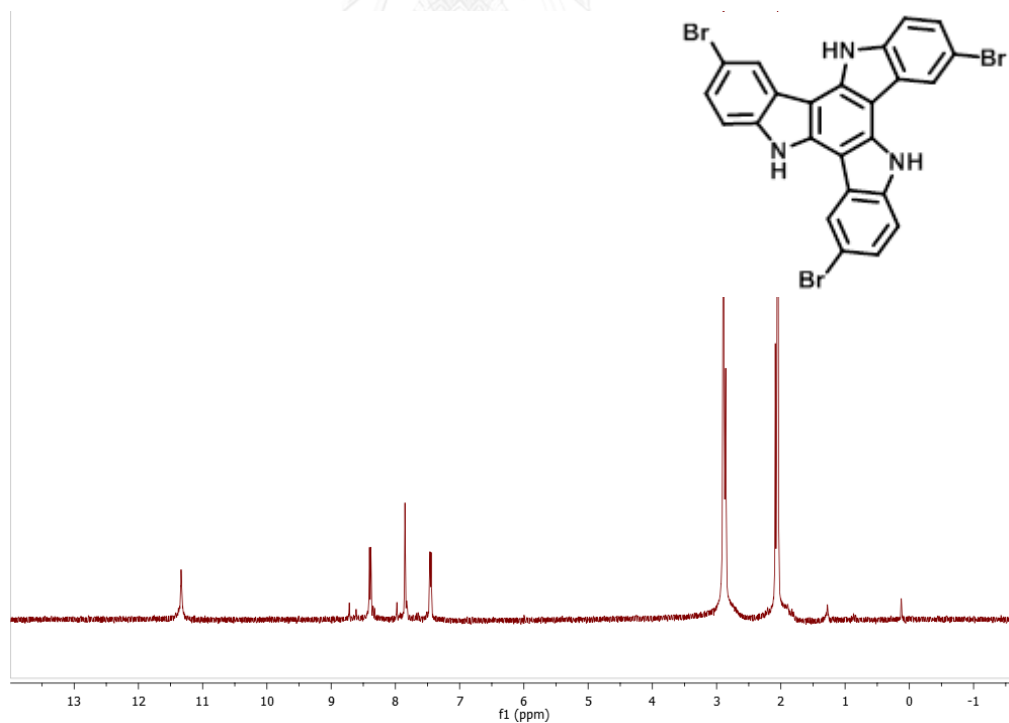
Figure A2. ¹H-NMR of 3,8,13-tribromo-10,15-dihydro-5H-diindolo[3,2-a:3',2'-c]carbazole in acetone-d6.
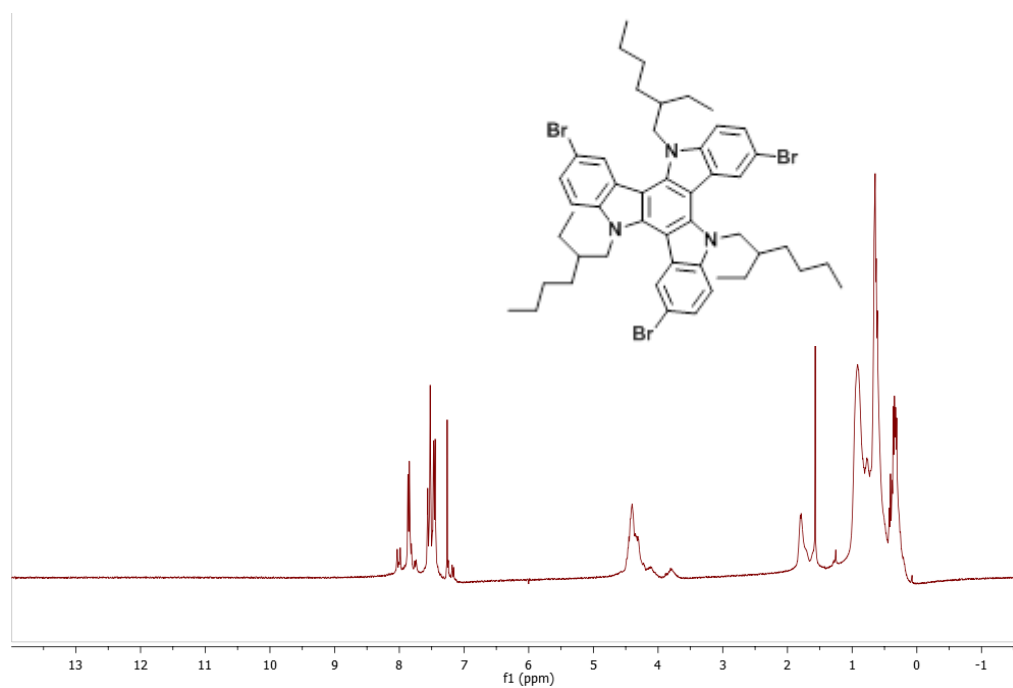
Figure A3. ^{1}H-NMR of 3,8,13-tribromo-5,10,15-tris(2-ethylhexyl)-10,15-dihydro-5H-diindolo[3,2-a:3',2'-c]carbazole in CDCl$_3$.
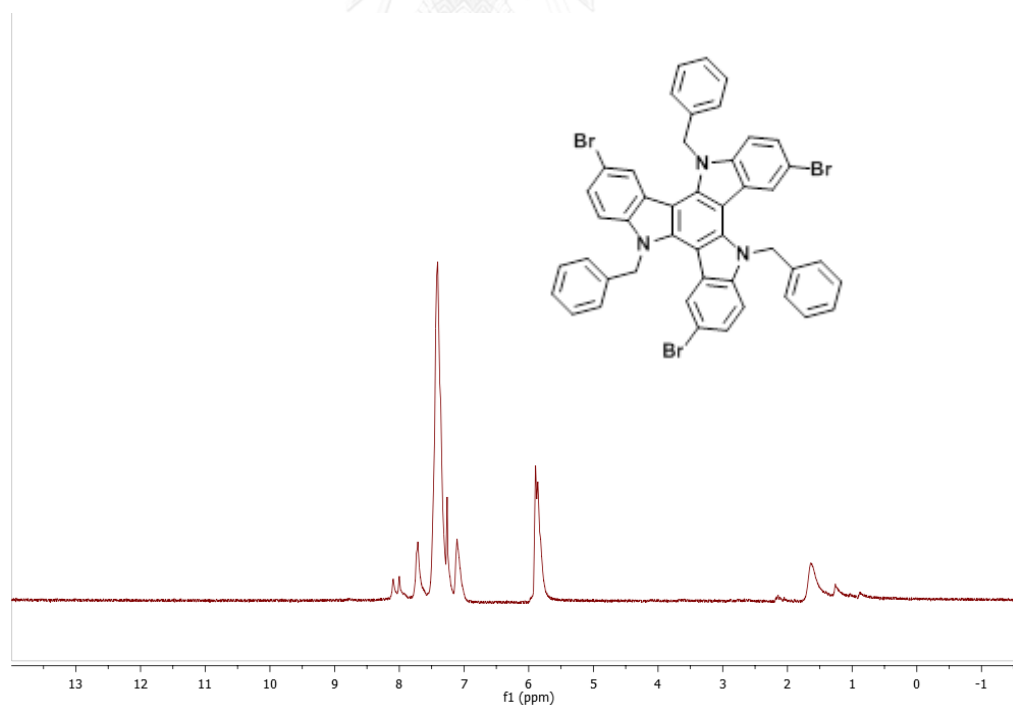
Figure A4. ^{1}H-NMR of 5,10,15-tribenzyl-3,8,13-tribromo-10,15-dihydro-5H-diindolo[3,2-a:3',2'-c]carbazole in CDCl$_3$.
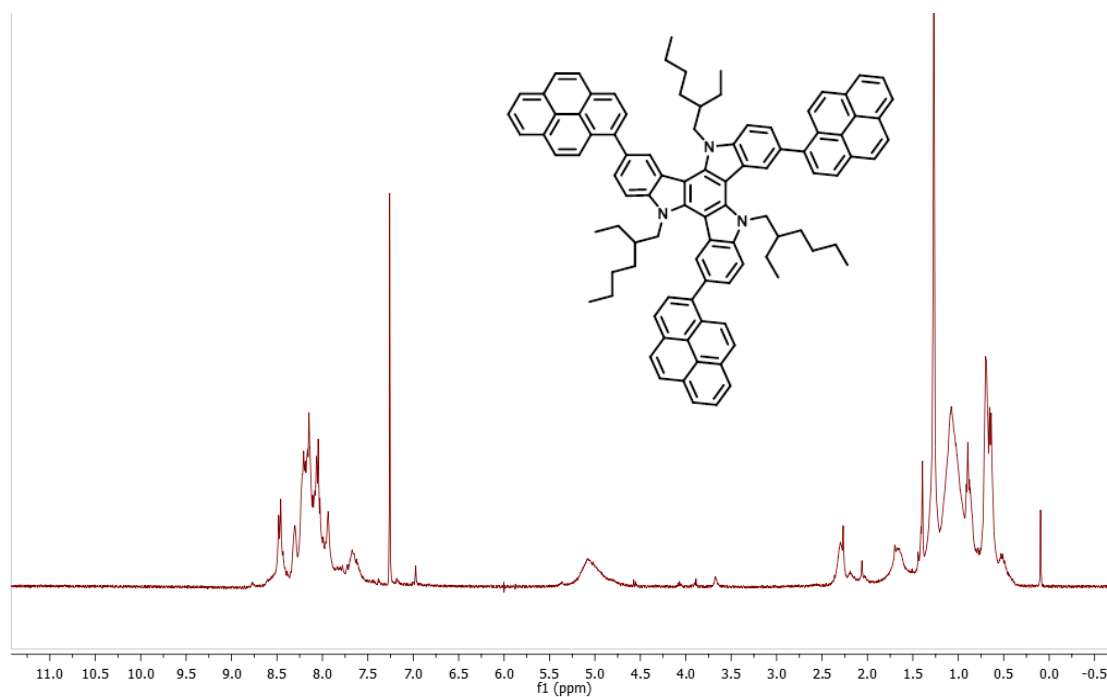
Figure A5. ¹H-NMR of 5,10,15-tris(2-ethylhexyl)-3,8,13-tri(pyren-1-yl)-10,15-dihydro-5H-diindolo[3,2-a:3',2'-c]carbazole in CDCl₃.
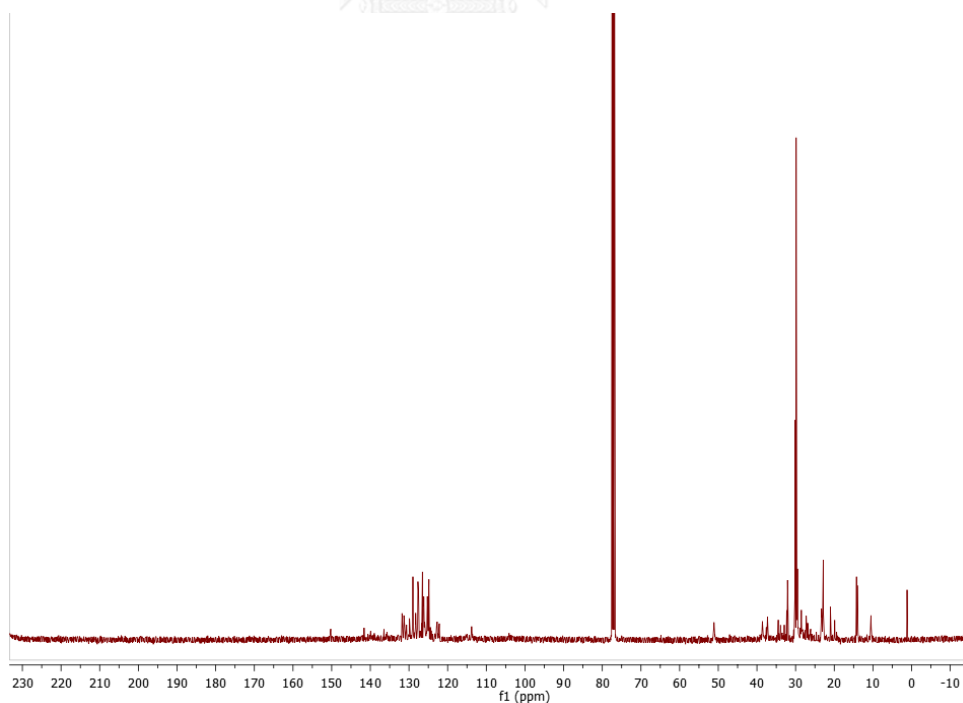
Figure A6. ¹³C-NMR of 5,10,15-tris(2-ethylhexyl)-3,8,13-tri(pyren-1-yl)-10,15-dihydro-5H-diindolo[3,2-a:3',2'-c]carbazole in CDCl₃.
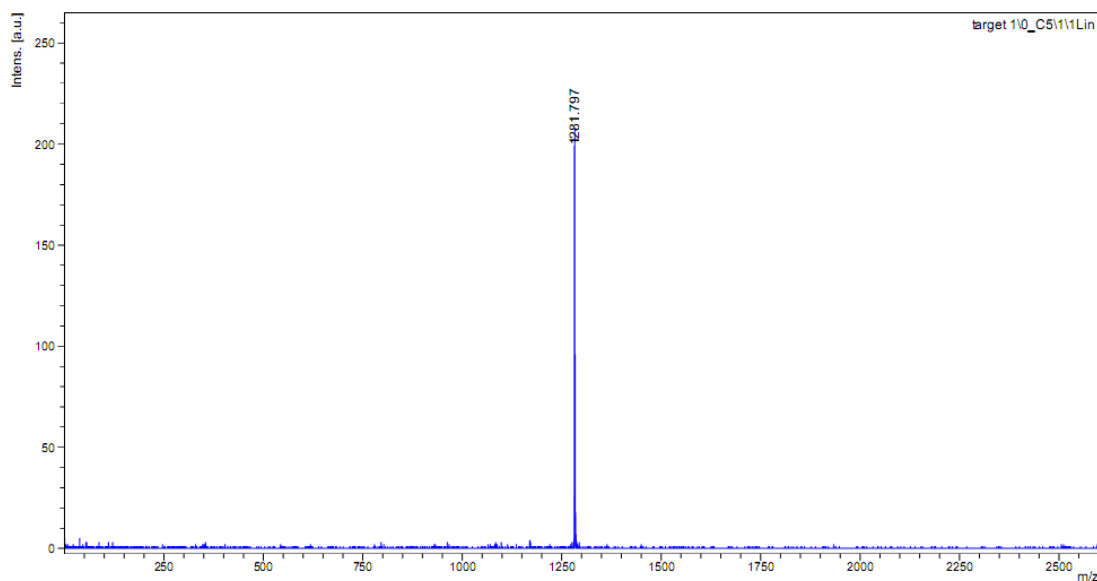
Figure A7. MALDI-TOF mass spectrum of 5,10,15-tris(2-ethylhexyl)-3,8,13-tri(pyren-1-yl)-10,15-dihydro-5H-diindolo[3,2-a:3',2'-c]carbazole.
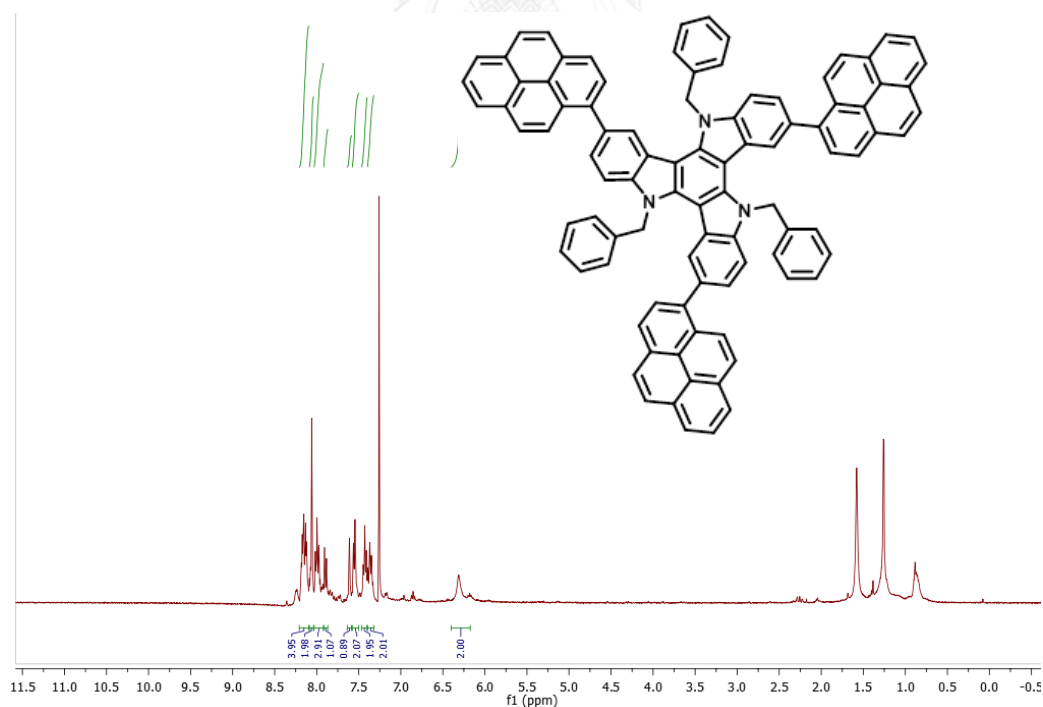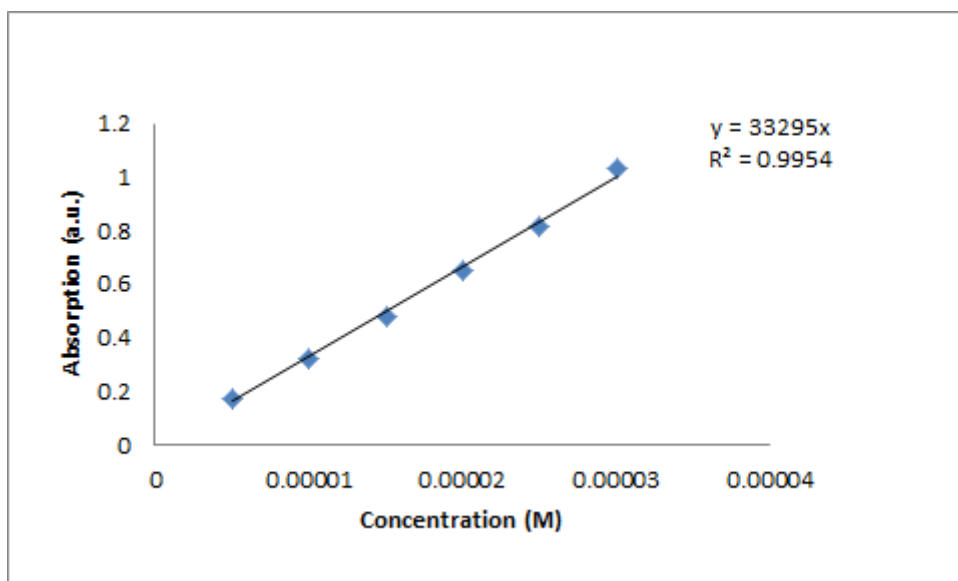

Figure A8. ^{1}H-NMR 5,10,15-tribenzyl-3,8,13-tri(pyren-1-yl)-10,15-dihydro-5H-diindolo[3,2-a:3',2'-c]carbazole in CDCl$_3$.
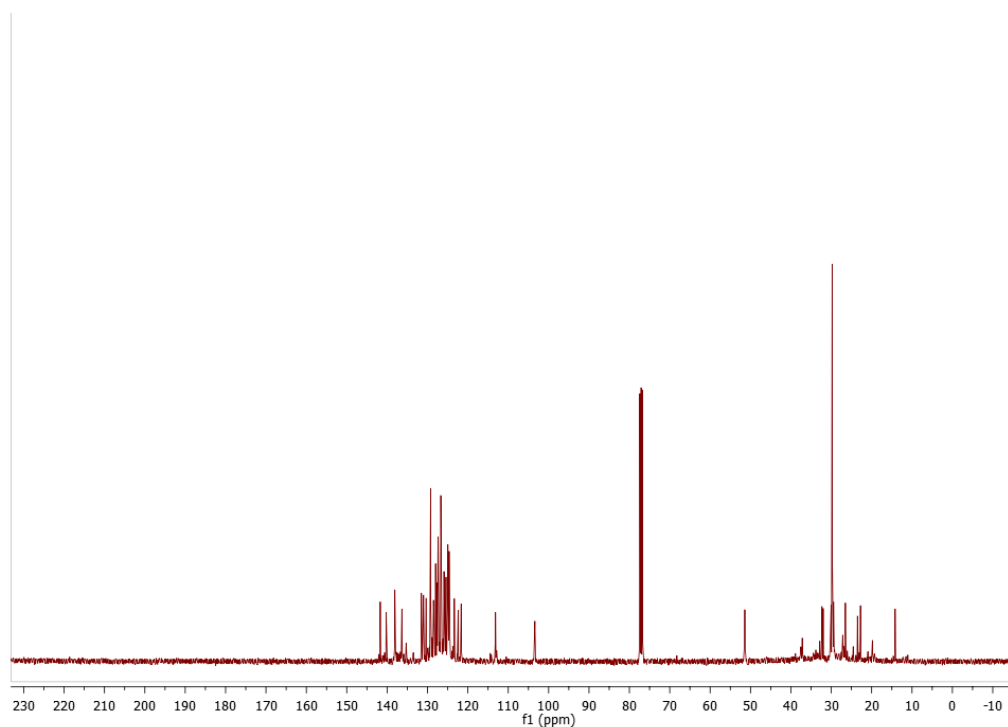
Figure A9. ^{13}C-NMR of 5,10,15-tribenzyl-3,8,13-tri(pyren-1-yl)-10,15-dihydro-5H-diindolo[3,2-a:3',2'-c]carbazole in CDCl$_3$.
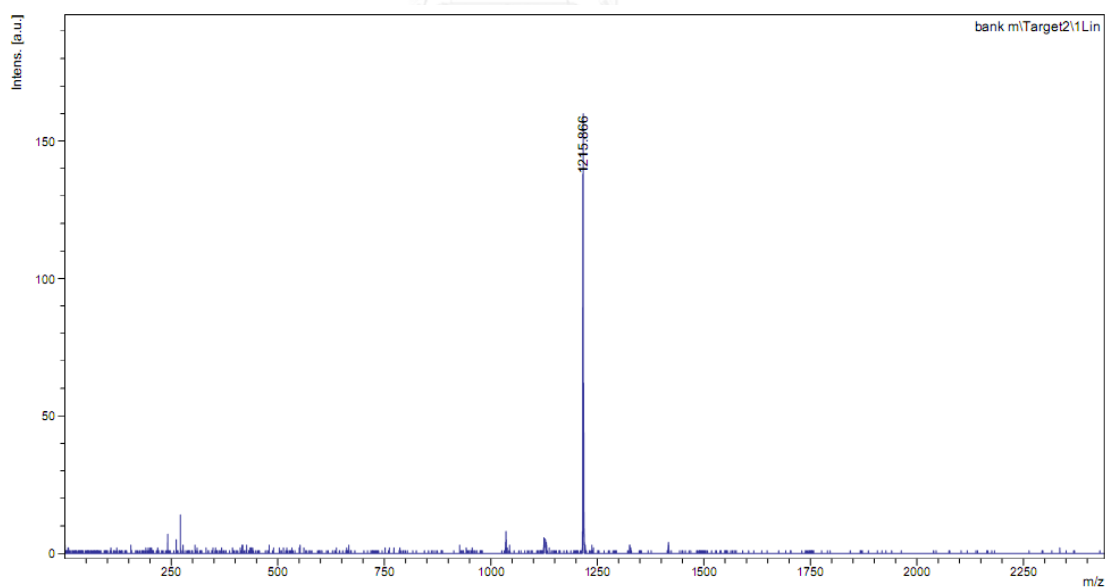
Figure A10. MALDI-TOF Mass spectrum of 5,10,15-tribenzyl-3,8,13-tri(pyren-1-yl)-10,15-dihydro-5H-diindolo[3,2-a:3',2'-c]carbazole.

Figure A11. Molarabsorption coefficient plot of TAT1 in $CHCl_3$.
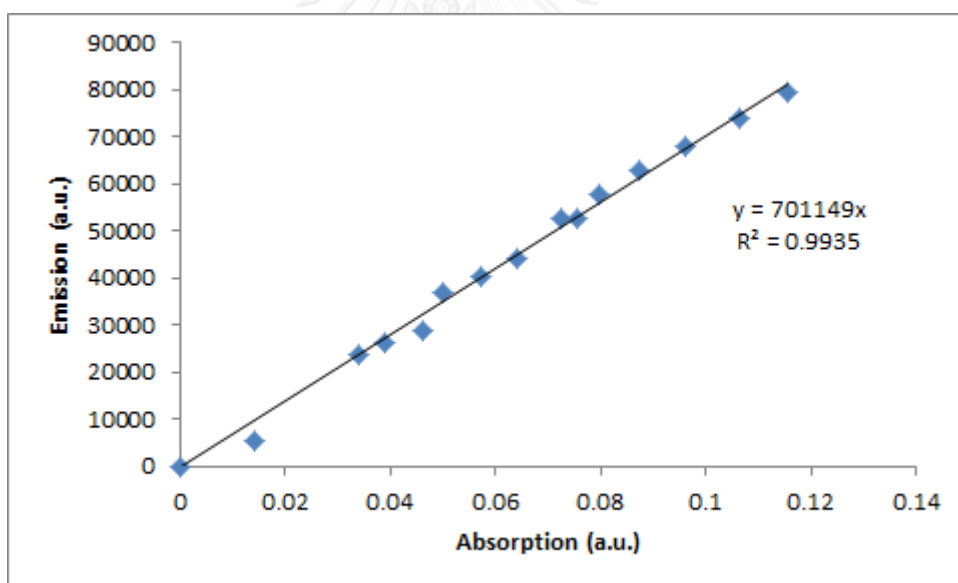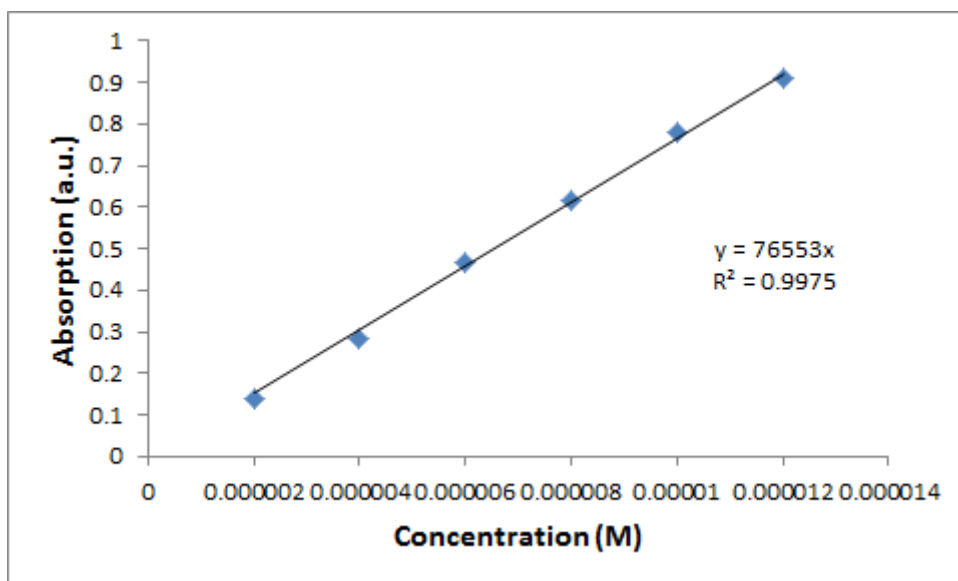

Figure A12. Quantum yield plot of TAT1 in $CHCl_3$.
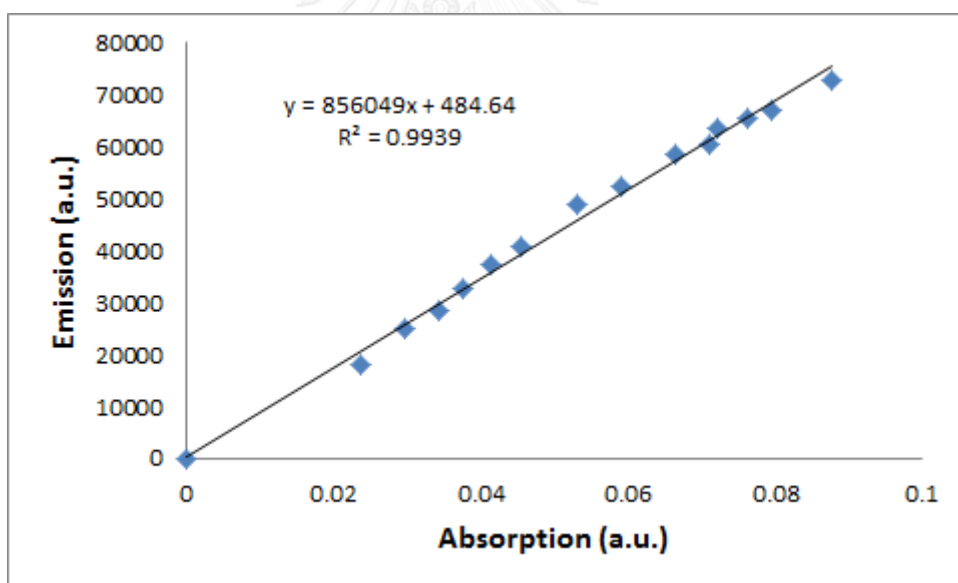
Figure A13. Molarabsorption coefficient plot of TAT2 in $CHCl_3$.
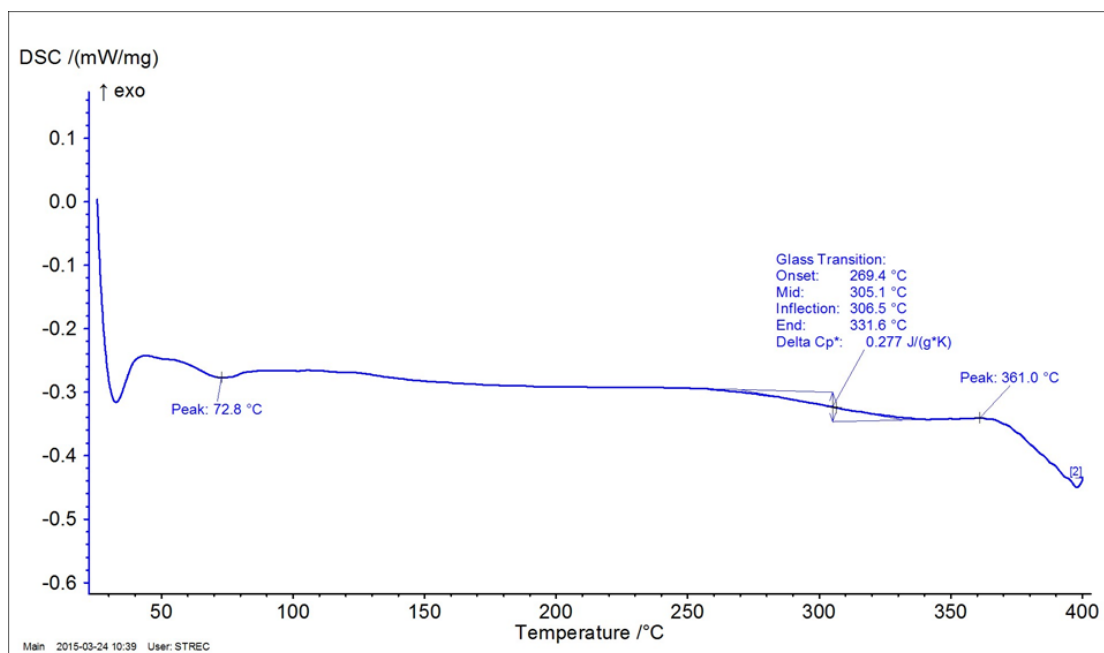

Figure A14. Quantum yield plot of TAT2 in $CHCl_3$.

Figure A15. DSC measurement of TAT1 with heating rate of 10°C per minute under N$_2$.
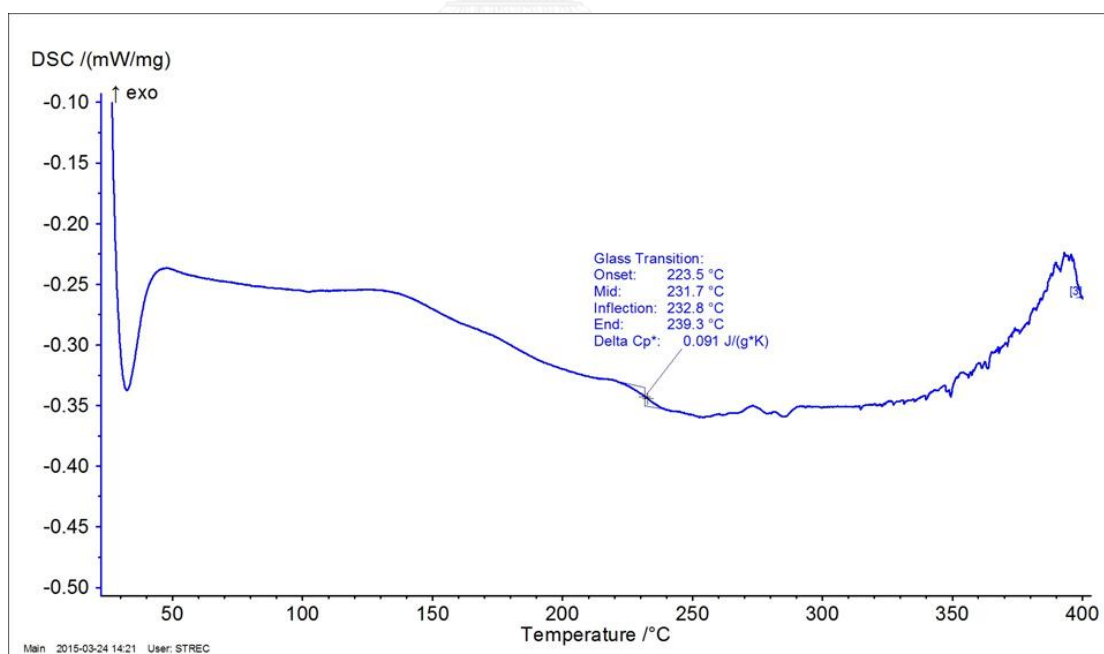

Figure A16. DSC measurement of TAT2 with heating rate of 10°C per minute under N$_2$.
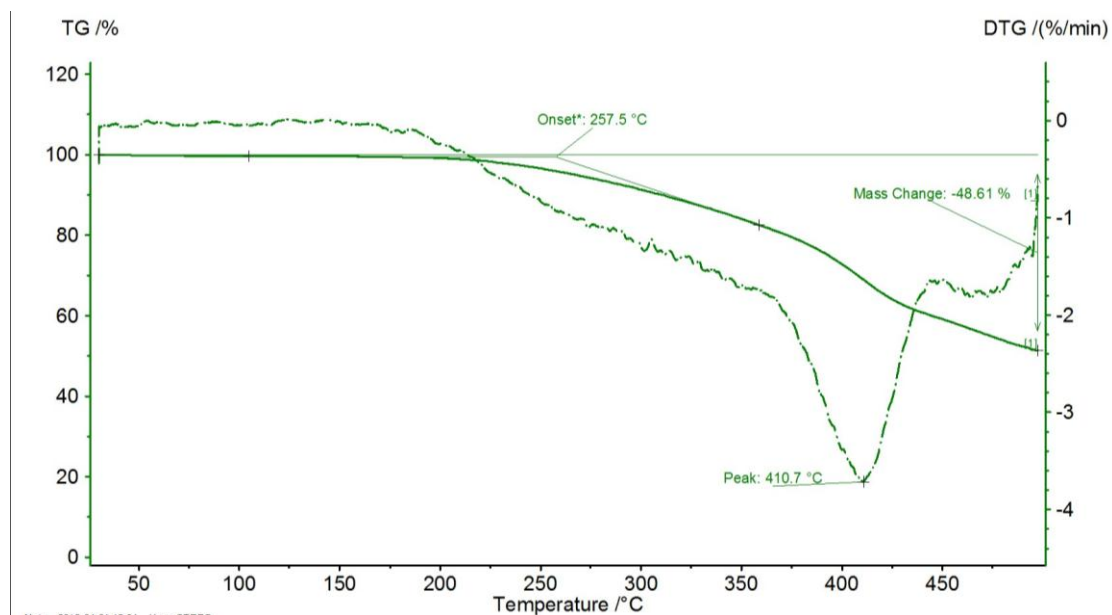
Figure A17. TGA measurement of TAT1 with heating rate of 10°C per minute under N$_2$.
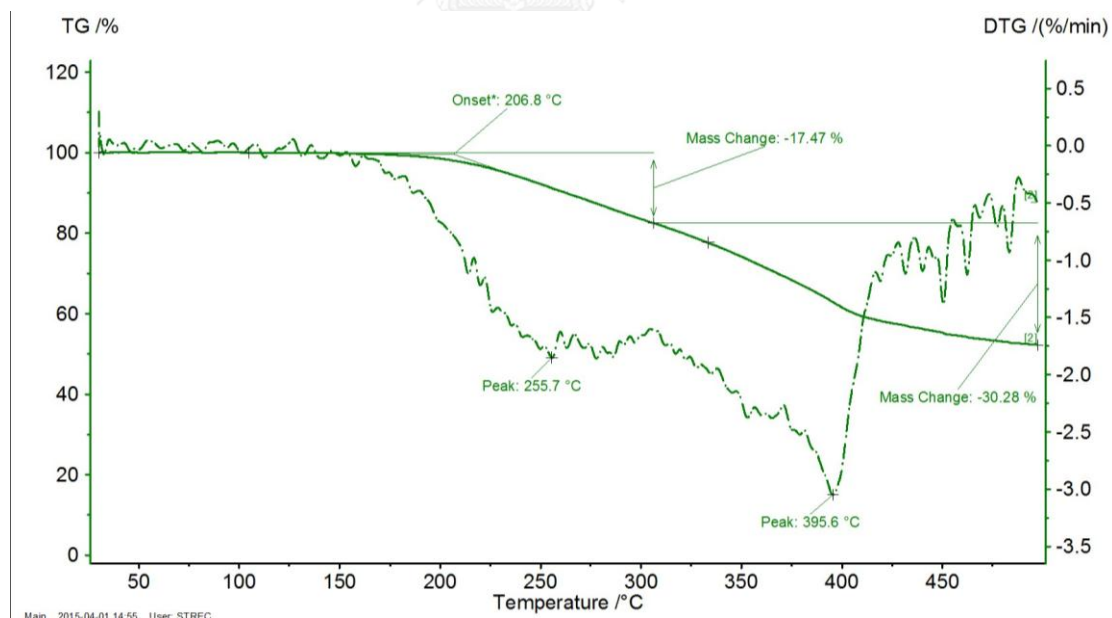

Figure A18. TGA measurement of TAT2 with heating rate of 10°C per minute under N$_2$.

VITA

Mr. Thanachart Techajaroonjit was born on December 17th, 1990 in Bangkok Thailand. He graduated with a Bachelor Degree of Science in Chemistry from Mahidol University in 2009. He pursued graduated study in the Master of Science Program at the Department of Chemistry, Faculty of Science, Chulalongkorn University, having carried out a thesis on synthesis and applications of triazatruxene in OLEDs. He can be contacted at 454 Soiratchada18, Ratchadaphisek road, Samsennok, Huaikhwang, Bangkok, 10310, Tel (087)-1641276, and email DSY_37738@hotmail.com.